Research Article | Vol. 16, No. 3 / 1 Mar 2026 / Optical Materials Express 662
Optical Materials EXPRESS

Pathway to versatile, point of care, and wearable photonics in the mid-infrared and fingerprint region based on quantum-cascade lasers and analytical and computational advances [Invited]

STEFANO TACCHEO,[1,2,*] THOMAS G. MAYERHÖFER,[3,4] MAEVA DORON,[5] MAXIME LEPAGE,[5] ROBIN DOUTÉ,[5] ALESSANDRA MANCA,[6] ALEXIS HOBL,[5] SONIA MESSAOUDENE,[5] MARION VOLPERT,[5] CHRISTOPHE CONSTANCIAS,[5] RICCARDO BALLARINI,[1] KÉVIN JOURDE,[5] JEAN-GUILLAUME COUTARD,[5] BERTRAND BOURLON,[5] ANTONIO D'AVOLIO,[2,6] BADHISE BEN BAKIR,[5] AND JUERGEN POPP[3,4]

[1] *Politecnico di Torino, DET-Department of Electronics and Telecommunication, Corso Duca degli Abruzzi 24, 10219 Torino, Italy*
[2] *Center for Biomarkers for Biophotonics – CiBiOF, 10129 Turin, Italy*
[3] *Leibniz Institute of Photonic Technology, Member of the research alliance "Leibniz Health Technologies," Albert-Einstein-Straße 9, 07745 Jena, Germany, Member of the Leibniz Centre for Photonics in Infection Research (LPI), Jena, Germany*
[4] *Friedrich Schiller University Jena, Institute of Physical Chemistry and Abbe Center of Photonics, Helmholtzweg 4, 07743 Jena, Germany, Member of the Leibniz Centre for Photonics in Infection Research (LPI), Jena, Germany*
[5] *Univ. Grenoble Alpes, CEA, LETI, MINATEC campus, F-38000 Grenoble, France*
[6] *University of Turin, Department of Medical Sciences, Laboratory of Clinical Pharmacology and Pharmacogenetics, Amedeo di Savoia Hospital, Corso Svizzera 164, 10149 Turin, Italy*
[*] *stefano.taccheo@polito.it*

Abstract: This paper aims to propose and discuss a pathway to versatile, portable, and wearable photonics devices in the mid-infrared region. We address the benefits and challenges of mid-infrared spectroscopy in the fingerprint region and the development of low-cost mass production devices for real-world applications in the near future. Firstly, the paper briefly introduces the mid-infrared and fingerprint region and discusses the importance of the detection of mid-infrared biomarkers for point-of-care medical applications, stressing the importance of multi-wavelength probing systems. We also discuss the challenge of long-wavelength signals through the matter and the benefits of photo-acoustic detection. The pathway we envisage is twofold: the first is to improve and predict deviation from the standard Bouguer–Beer–Lambert approximation for light propagation in tissue and matter. This approach requires calibrated and wavelength-specific sources. Secondly, to address these requirements, the paper presents the potential for future low-cost personalized devices based on an array of quantum cascade lasers developed on low-cost C-MOS technology and using photo-acoustic detection. The technology was first developed for gas analyses, but we report on a recent successful wearable device for glucose monitoring, which passed clinical trials. This technology will allow the development of future widespread portable mid-infrared devices with potential application not only in healthcare, addressed here, but also in precise gas and environmental chemical monitoring. The ability to record mid-infrared biomarkers at the point of care will be fundamental for the personalized optical digital twin, which will be the cornerstone of future healthcare systems.

#580918 https://doi.org/10.1364/OME.580918
Journal © 2026 Received 3 Nov 2025; revised 5 Jan 2026; accepted 7 Jan 2026; published 24 Feb 2026

Optical Materials EXPRESS

1. Introduction

The Mid-Infrared (MIR) wavelength interval extends from 3 microns to 50 microns following the Internation Organization for Standardization definition [1], yet in chemical spectroscopy if often defined between 2.5 microns and 25 microns. Whatever the chosen definition is, MIR is a spectral region of the utmost importance for spectroscopy. In this spectral range, complex structures or even molecular species exhibit specific vibrational absorption bands with large extinction coefficients. Hence mid-IR spectroscopy potentially provides extremely sensitive chemical analysis. This wavelength interval includes the so called "fingerprint region" (above about 6.7 micron or below 1500cm^{-1}). It is the region in which even two isomers exhibit different absorption and emission patterns due to the different vibrational modes (defined by the different three-dimensional organization of the very same type and number of atoms) [2].

This difference is due to the fact that any change in a molecule three-dimensional arrangement changes the vibrational mode frequencies and amplitudes and therefore provides a unique pattern that allows us to recognize even a specific isomeric structure. For this reason, MIR spectra offer molecular fingerprints of numerous gases, liquids and solids such as greenhouse gases, ground, water and air pollutants, pharmaceuticals, toxic agents, oil, oil products and plastics, biological tissue and many others [4–7].

Figure 1 highlights the potential as well challenges related to MIR spectroscopy. Figure 1 shows the absorption spectra of two isomers: the propan-1-ol ($CH_3CH_2CH_2OH$) and propan-2-ol ($(CH_3)_2CHOH$), and atmospheric absorption. Up to above 6.5 microns the absorption spectra of the two isomers are almost identical while between 6.5 microns and 12 microns are completely different due to the different structure and vibrational modes, providing a unique fingerprint interval with strong absorption peaks at different wavelengths. However, since all substances have vibrational modes as soon as the target substance is embedded in a medium, here air but can be serum or blood, or simply investigated under a surface, there is a huge overlap with environmental absorption, which is often at a concentration several order of magnitude higher. Therefore, even a far lower medium absorption coefficient origins a far higher absorption than target substance. In addition, the signal extraction is also quite difficult due to environmental absorption or scattering, see section three for a deeper analysis, and this prevents the use of low power and single wavelength probe. Spectroscopy based on markers at several wavelengths is therefore the most effective.

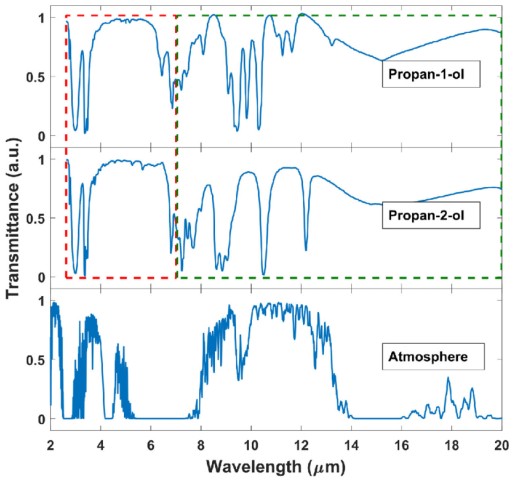

Fig. 1. Absorption Spectron of two isomer gases Propan-1-ol and Propan-2-ol and the atmospheric absorption. Reprinted with permission from Ref. [3].

Optical Materials EXPRESS

We focus the paper on medical application of Mid-infrared spectroscopy [7] as one of the most promising applications of wearable and portable MIR devices. For example, in the field of chronic illnesses such as chronic obstructive pulmonary disease (COPD) [8] and viruses like Zika [9], Hepatitis B and C [10] and Sars-CoV-2, samples [11] have been analyzed using MIR and THz spectroscopy in Laboratory environmental looking at specific absorption patterns in serum or blood samples. In fact, the presence of an illness can alter the components of serum or blood and their vibrational modes intensity [9,10]. Another possibility is to look at changes in vibrational modes of probes substances. Figure 2 shows how N, Cl-doped carbon (N,Cl-CD) dots optical properties in the fingerprint region may change if vancomycin, a glycopeptide antibiotic, is present. Vancomycin has affinity for Staphylococcus aureus and the attachment of the virus to the N,Cl-CD@van modifies the fluorescence, Specific vibrational spectral features that can be therefore used as a probe of Staphylococcus aureus presence [12]. The group of one of the authors has also been able [13] to detect and discriminate Covid-like viruses from other types of viruses, by using a femtosecond laser system.

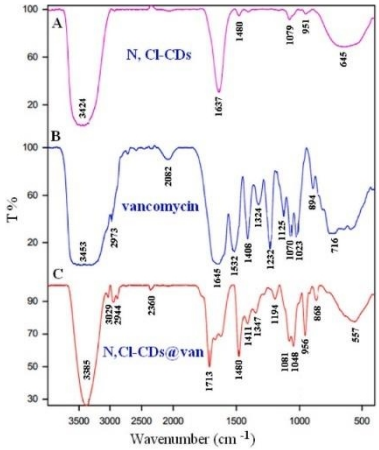

Fig. 2. FTIR spectra of A) Carbon Dots, B) vancomycin, and C) Carbon Dots@vancomycin. Reprinted with permission from Ref. [12]

However, all above results were laboratory-based investigation and on very expensive probe equipment [13] and/or very sensitive scanning Fourier-transform infrared (FTIR) interferometers [8–11] using broadband sources to probe at different wavelengths. Broadband excitation sources are based either on a low power density thermal emitter or, more efficiently and powerfully, on supercontinuum generation [14,15]. In alternative FTIR/Raman spectroscopy is available but it loses the ability of more specifically excite the target substance. In all cases the wavelength selective element is usually a high-resolution Fourier-Transform monochromator to provide enough signal-to-noise ratio due to low probe spectral power, which is so far complex and expensive and therefore difficult to move from a laboratory and not suitable in terms of cost and footprint for wearable photonics.

To try to develop compact devices extending capabilities from visible and IR to the MIR [16,17] there are several possibilities, however since we deal with the fingerprint region we do not consider technology such as silicon photonics platforms since they are usually limited in wavelength [18]. Even if measurements show one can work up to 7 μm with high index contrast platform, including the combination of Silicon and Silicon Nitride, this technology does not cover the main part of the fingerprint region [19]. We briefly mention here other technologies which are still in their infancy but can offer interesting functionalities in future. Detectors and imagers are a very promising field for flexible photonics but yet at the initial stage [20,21],

Optical Materials EXPRESS

more recently black phosphorus-based technology demonstrated quite interesting results for mid-infrared applications [22–25]. A further technology to mention is Mid-infrared Plasmonic with a set of applications and benefitting from the ability of tuning the resonance using several materials including phase-change materials [26,27]. Flexibility can be achieved using their compatibility with flexible substrates. Plasmonic resonance applied to microfluidic devices was also investigated for biomedical application such as the diagnosis of neurodegenerative disorders in clinical environmental [28] and discuss later in section two.

Therefore, it is of the utmost importance to develop highly reliable real-world low-cost wearable/portable devices eliminating the above limitations. With this respect Quantum-Cascade-lasers (QCLs), which are based on transitions between electronic sub-bands due to quantum confinement in a semiconductor heterostructure [29,30], are very interesting probe sources. Room temperature was demonstrated only quite recently [31] and now they offer multimode, single-frequency and tunable emission [32–34], while mode-locked operation [35] paved the way to comb generation [36]. Their high-power spectral density with respect to any broadband source joined to the ability to excite a specific absorption peak of the target substance makes them ideal for spectroscopy. QCLs can be integrated with other functionalities [34,37], and several fabrication methods have been investigated [31,34,38].

However, to fully address the requirement of biomarkers detection using wearable/portable devices a low-cost integration-enabling process for mass production of array of QCLs is required. It was recently demonstrated, by some of the authors, the possibility of transferring the fabrication process of QCLs on a 200 CMOS pilot line [39]. This technology has also two significant advantages with respect to broadband source-based systems: first it provides far higher power at desired probe wavelengths, second it removes the necessity of a large and costly wavelength selective detector. Within this framework wearable device for biomarker monitoring based on QCLs has been studied [40] and a device for glucose monitoring [41] successfully went through clinical trials. A Glucose device long term monitoring is important not only for diabetes but is also fundamental for getting insight in glucose-level relationship with adrenal insufficiency therapy and crises [42,43]. This highlights the potential of non-invasive wearable medical devices for medical advancements.

This technology offers reliable set of stable wavelengths which fits the spectral wavelength of interest and may also enable improved analytic and computational analysis of propagation of MIR radiation into tissues and materials and of the possible deviations from standard Bouguer–Beer–Lambert (BBL) Law. These refined analyses will further enhance the suitability of MIR wearable photonics for biomedical applications including clinical trials.

In this paper we propose a comprehensive pathway to wearable and portable cost-effective MIR photonics devices for biomedical applications. The focus is on two main approaches to improve device compactness and sensitivity. In section two we discuss the need of multiple wavelengths for detections while in section three the paper discusses deviation from the standard Bouguer–Beer–Lambert approximation for light propagation in tissue and matter in order to further improve measured data analyses. In section four the paper presents and discusses low-cost personalized devices based on an array of Quantum Cascade Lasers developed on low-cost C-MOS technology and using photo-acoustic detection. The technology is first discussed for gas analyses and later we report on a recent successful wearable device for glucose monitoring. We also remind that in most cases to extract a signal with strong background noise a large amount of Machine Learning (ML) [22] and Artificial Intelligence (AI) [28] post processing [44,45] is required. Computation load and use of ML and AI will be briefly discussed in the following sections.

We believe this technological approach will pave the way for the development of future cost-effective wearable and portable Mid-infrared devices with potential application not only in healthcare but also in precise gases and environmental chemical monitoring. The ability in

Optical Materials EXPRESS

non-invasive long-term recording Mid-infrared biomarkers at point-of-care will be fundamental for the future Personalized Optical Digital Twin, which will be the cornerstone of future healthcare systems.

2. Mid-infrared biomarkers

2.1. State of art

This section we discuss the importance of being able to detect MIR biomarkers and in particular the benefit of been able to use wearable and portable devices. The recent advances in healthcare biomarker detection have notably featured photoacoustic- and mid-infrared, based technology due to their sensitive, non-invasive, and real-time diagnostic characteristics [44,46]. These technologies can revolutionize diagnostics, monitoring, and personalized treatment in healthcare and are necessary for efficient PODT [47,48].

Photoacoustic imaging technology offers elevated spatial resolution and deep tissue penetration, providing functional and molecular information [49]. For these reasons, it has been used in cancer management with recent improvements such as dynamic modelling of sensor data for automated blood sample classification and drug delivery monitoring [50–52]. These sensors allow precise assessment of physiological changes and personalized therapy monitoring in clinical practice, paving the way for point-of-care diagnostics [53]. In details, photoacoustic imaging shows high specificity in hemoglobin, melanin, and lipids, as well as drugs and exogenous contrast agent determination, for applications including tumor mapping, inflammatory status, and vascular monitoring [49,54].

These biomarkers shed light on tissue structures, functions, and pathological conditions with great tissue penetration and molecular sensitivity [55–57]. Digital and photonic biomarkers, when combined with AI, represent the forefront of precision diagnostics and enable real-world, personalized disease management [58,59]. For example, nanostructured photoacoustic probes have been utilized to detect bacterial infections by targeting specific enzymatic activities or membrane components, providing insights into pathogen localization and antibiotic response [60].

In recent years MIR sensor technologies, based on, plasmonic and nano plasmonic metasurfaces-based, have been developed for the detection of protein biomarkers, in particular between 2.5- 20 micron (wavenumber between 500 cm^{-1} and 4000 cm^{-1}), for example in chronic kidney diseases [46,61]. The high reproducibility and specificity of this technology, coupled with machine learning, allow for early diagnosis and personalized disease treatment [62]. However, while plasmonic and nano-plasmonic offer significant properties still the detection and probe require the use of expensive and lab-based FTIR or attenuated total reflectance (ATR) spectroscopic analyses [63]

The capacity to identify protein biomarkers, oligomeric and fibrillar aggregates, and to perform simultaneous monitoring of multiple disease-associated biomarkers makes these technologies extremely encouraging for early diagnosis and monitoring of complex pathologies such as Alzheimer's and Parkinson's [64]. Biomarkers related to chronic diseases including hypertension, dyslipidaemia, and diabetes can be identified by this technique: it is a promising tool for early disease detection and health monitoring thanks to its high reproducibility and non-invasive nature [62,63,65,66]. Cardiovascular research is based on multi-biomarker panels made possible by MIR technologies, which can detect inflammatory markers, microRNAs, and proteins. These panels aim to find early-stage disease and predict acute cardiovascular events before symptoms appear clinically. Moreover, the development of portable and wearable FTIR-based sensors has made continuous patient monitoring possible [67,68]. Most studies applied benchtop FTIR instruments with ATR accessories for serum or plasma analysis, while recent works explored portable mid-IR devices for point-of-care use.

Optical Materials EXPRESS

Mid infrared FTIR/ATR spectroscopy has been used to analyse biofluids for molecular fingerprints characteristic of viral and bacterial infections. These techniques enable rapid respiratory infections screening, identifying metabolic and proteomic alterations associated with host response [62]. Plasma and interstitial fluid can be analysed, highlighting alterations in metabolic profiles related to endocrine pathologies.

2.2. Mid-infrared wearable sensors for non-invasive biomarkers monitoring

As mentioned previously, MIR spectroscopy exhibits major advantages over traditional biomarker detection methods in other wavelength intervals, providing a unique 'fingerprint' for an extensive range of biological molecules [69]. Unlike other methods (e.g. Polymerase Chain Reaction or Enzyme-Linked Immunosorbent Assay), that target specific analytes, MIR captures the entire biochemical profile of a sample without needing labels or considerable sample preparation. This allows a fast, multiplexed and simultaneous detection of multiple biomarkers, essential for diagnosis and personalized treatment.

Moreover, MIR spectroscopy is able to differentiate minimal molecular changes that occur in disease states, often at an early stage. For example, in cancer diagnosis, MIR has been used to discriminate tumour tissue from healthy tissue based on their spectral differences, detecting minor biochemical alterations before morphological changes become evident [70]. In the context of neurodegenerative diseases like Alzheimer's, MIR identifies protein aggregates and fibrils, providing early biomarkers that are difficult to detect with traditional technologies [6].

In addition, MIR can analyse different matrices such as blood, urine, or saliva with little or no preparation, allowing fast, point-of-care testing [71]. This offers significant clinical benefits, especially for continuous monitoring or in resource-limited settings.

In light of these evidences, different MIR-based portable devices have been developed to improve in situ and real-time measurements without sample preparation [72] and allow to probe vibrational modes [7,18] present in various proteins, lipids, and other crucial biomarkers [73] with compact devices [18]. Applications include monitoring molecules, like glucose and ketone bodies, albumin or even drugs, enabling early diagnosis, therapeutic drug monitoring, and chronic disease management with great accuracy [74].

As an example, vancomycin, a glycopeptide antibiotic, shows specific vibrational absorption bands in the mid infrared spectrum, particularly a global shift of the amide I band around 1665 and 1689 cm^{-1}, weak shoulders can be observed below 1665 cm^{-1}. These spectral fingerprints make possible precise vancomycin identification and mapping in biological tissues, revealing heterogeneities in deposits due to drug interactions with cellular components [75].

MIR-based technology can be applied also in the field of biospectroscopy to identify cell types based on characteristic biomarkers. For example, Fig. 3 shows cervical cells characteristic vibrational pattern, which is labelled as follows: Amide I (~1650 cm-1), Amide II (~1550 cm-1), Amide III (~1260 cm-1), carbohydrates (~1155 cm-1), glycogen (~1030 cm-1), lipids (~1750cm-1), symmetric phosphate stretching vibrations (vasPO2 -; ~1225 cm-1), symmetric phosphate stretching vibrations (vsPO2 -; ~1080 cm-1), protein phosphorylation (~970 cm-1) [76].

MIR vibrational spectra of hepatitis infected serum samples vs. not infected show defined peaks, as reported in Fig. 4, highlighted by the bands that have been used for hepatitis diagnosis and monitoring [10].

An example of portable sensor to monitor metabolic syndrome biomarkers is the MiWear. This wearable mid infrared sensor is able to non-invasively monitoring key biomarkers in the interstitial fluid just beneath the skin. It uses a miniaturized mid-infrared spectrometer, based on advanced Quantum Cascade Laser technology, to emit mid infrared light across specific wavelengths corresponding to vibrational absorption bands of clinically relevant biomolecules, as uric acid, albumin, ketone bodies, and other metabolites associated with metabolic syndrome [40]

Optical Materials EXPRESS

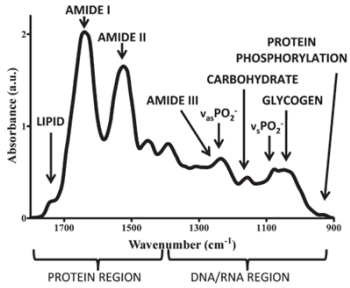

Fig. 3. labelling of vibrational modes in the FTIR spectrum of cervical cells. Reprinted with permission from Ref. [76].

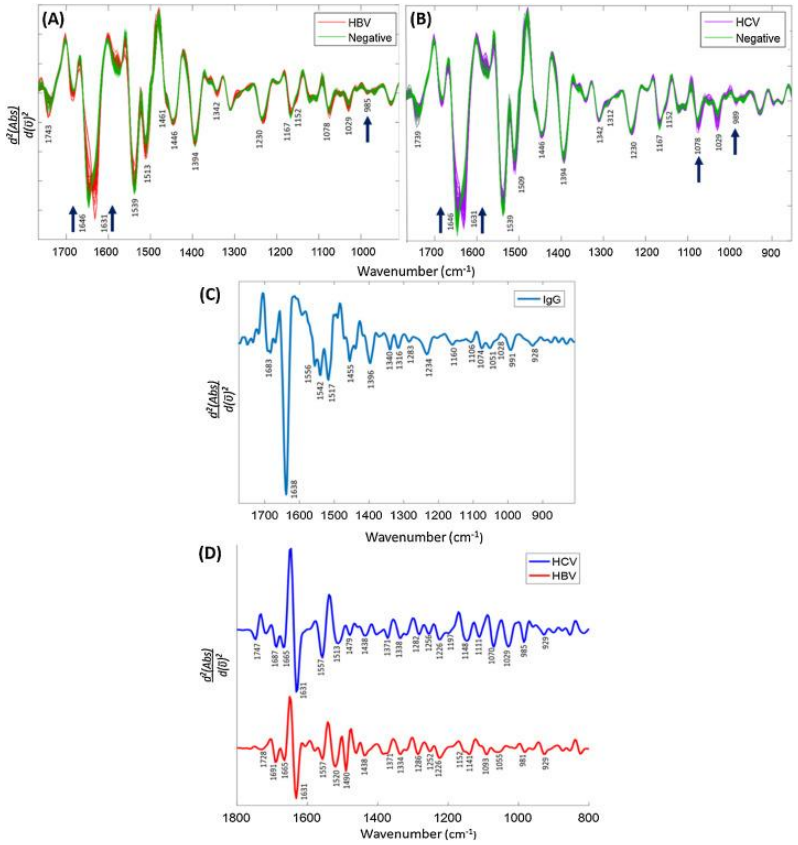

Fig. 4. Normalized spectra of A). HBV vs negative samples, B). HCV vs negative samples, C). IgG D). Mean control (negative) subtracted from mean of HCV (blue) and HBV (red), respectively. Reprinted with permission from Ref. [10].

Optical Materials EXPRESS

2.3. Mid-infrared and photoacoustic sensors for therapeutic drug monitoring

One of the most important applications is therapeutic drug monitoring (TDM), which is crucial across multiple clinical domains, oncology and neurodegenerative diseases, cardiovascular disease, endocrinology, and infectious diseases, optimizing efficacy and minimizing toxicity. TDM is the clinical tool which measures drug levels in patient bloodstream, optimizing the individual dosage regimens. It allows to use difficult-to-manage drugs with narrow therapeutic ranges, optimizing the clinical outcome in patients [77].

The quantification of drugs and their metabolites in biological matrices such as blood, plasma, urine, or tissues is crucial for pharmacokinetic and pharmacodynamic studies, drug development, TDM, and personalized medicine. Emerging photoacoustic and MIR sensor technologies offer advances in non-invasive, real-time, and highly sensitive measurement of drug levels [78,79].

The high sensitivity of MIR sensors has been used to track neuroprotective and symptomatic drugs such as acetylcholinesterase inhibitors or dopamine agonists in neurodegenerative diseases. MIR spectroscopy of biofluids recognizes molecular fingerprints associated with therapeutic drug levels and disease progression, enabling personalized treatment. Meanwhile, photoacoustic nanoprobes targeting specific biomarkers provide imaging-guided tracking of drug delivery across the blood-brain barrier, offering insights into pharmacokinetics within neural tissues [80].

In endocrinology, both photoacoustic and MIR technologies enable monitoring of hormonal therapies, including insulin and thyroid medications. Photoacoustic sensors detect plasma drug concentrations and metabolic changes at the tissue level, enabling personalized adjustment of dosages in diabetes and thyroid dysfunction. MIR spectroscopy of interstitial fluids combined with biophotonic hormone sensors allows continuous glucose and hormone level monitoring in real time, enhancing management of chronic endocrine disorders [81,82].

For infectious diseases, TDM using photoacoustic sensors enable rapid and label-free quantification of antiviral and antibiotic drugs in blood and tissues, crucial for acting against resistance and ensuring therapeutic efficacy. Photoacoustic molecular probes track drug accumulation and metabolism at infection sites, facilitating dynamic adjustments based on pathogen response. Mid infrared biosensors analyse metabolic alterations in patient biofluids, providing indirect but timely feedback on antimicrobial therapy effectiveness [77].

These advances in photoacoustic, and MIR platforms promise to revolutionize TDM by enabling precise, timely, and non-invasive dosing optimization personalized to patient pathophysiology across diverse clinical fields [48,78,83], and will be the cornerstone for the future Personalized Optical Digital Twin concept, as better discussed in the following section.

3. From the Beer-Lambert law to the optical twin: analytical and computational pathways in wearable MIR photonics

3.1. Beer–Lambert law in wearable mid-IR photonics

In this section, we focus on the necessity of accurate and physically consistent models to describe the interaction of light with tissue and biological matter. The quantitative analysis of infrared spectra is historically rooted in the Bouguer–Beer–Lambert (BBL) law, a formulation both elegant and deceptively simple. Its development spans more than a century: Pierre Bouguer observed in 1729 that light attenuation in an absorbing medium follows an exponential dependence on path length [84]. Johann Heinrich Lambert generalized this in *Photometria* [85], formalizing the relation between intensity and layer thickness, and August Beer extended it in 1852 by introducing concentration as a variable [86]. Together, these contributions led to Eq. (1), which represents the attenuation of light intensity and is familiar to every spectroscopist [87]:

$$-\log_{10}\frac{I}{I_0} = A = \varepsilon \cdot c \cdot d \tag{1}$$

Optical Materials EXPRESS

where absorbance A depends linearly on the molar absorption coefficient ε, the concentration c, and the path length d.

This apparently simple relation revolutionized analytical chemistry. Long before electronic detectors, it enabled quantitative assays using only visual estimates of transmitted light. Its power lay in its accessibility: a single measurement could be read as directly proportional to the amount of substance. For this reason, the BBL law remains the default framework of infrared spectroscopy, underpinning classical least squares, partial least squares regression, and many calibration models [88].

Its limitations, however, were recognized early. Beer already corrected for reflection losses using Fresnel's equations [89]. Maxwell's electromagnetic theory reframed absorption as a wave–matter interaction governed by the dielectric function [90], while Lorentz showed that molecules experience both the external field and the influence of neighboring dipoles [91,92]. Planck demonstrated that strong oscillators deviate from the linear response predicted by the BBL law, their band shapes modified by collective interactions [93]. These refinements established that the BBL law is not fundamental physics but an approximation valid only for weak absorption, weak coupling, optical homogeneity, and negligible scattering. Later treatments, such as in Born and Wolf's *Principles of Optics*, fully embraced the wave-optics description [94].

The law remains relevant today because wearable and flexible mid-infrared (MIR) devices for preventive healthcare are still based on its central premise: absorbance scales with concentration. Non-invasive glucose monitoring, for example, assumes that the intensity of glucose-related bands in interstitial fluid correlates linearly with blood glucose levels [95]. Similar reasoning guides sensors for tumor metabolites, drugs, or volatile organics, where quantitative success depends on maintaining proportionality between concentration and spectral response.

However, these applications often operate in regimes where the BBL assumptions no longer hold. Biological tissues are heterogeneous, anisotropic, and strongly scattering. Hydration levels fluctuate, altering both baseline and band shapes. Device geometries involve bending, layered substrates, and attenuated total reflection (ATR) configurations that modify the optical field in ways simple linear models cannot capture. Uncorrected, such deviations obscure quantitative evaluation and are particularly problematic in preventive healthcare, where the goal is to detect subtle early biochemical changes rather than established disease. We propose a pathway to enhance light detection for wearable photonic systems as summarized in Fig. 5.

Several classes of deviations can be identified, each reflecting a different physical mechanism that causes departures from Beer–Lambert behavior.

3.1.1. Interference and standing waves

When light interacts with layered structures—polymer coatings, skin layers, or thin films—multiple reflections create Fabry–Pérot resonances. These fringes redistribute the local electric field, so the apparent molar absorption coefficient fluctuates with layer thickness or substrate properties, even at constant concentration. A polymer layer on CaF_2 can show intensity variations of ±20% purely due to interference [96].

3.1.2. ATR-specific effects

ATR introduces characteristic deviations from Beer–Lambert scaling. Often described by evanescent fields, ATR absorption is better understood as reflection minus transmission into an absorbing medium [97]. Once absorption occurs, field intensity varies smoothly with incidence angle and absorption index, without discontinuities at the critical angle. Strong bands are therefore shifted and distorted relative to transmission spectra, and polarization further amplifies deviations. Correction models based on "effective thickness" are valid only for weak absorbers and fail for strong oscillators such as carbonyl or amide bands [96,98–103]. In layered systems,

Optical Materials EXPRESS

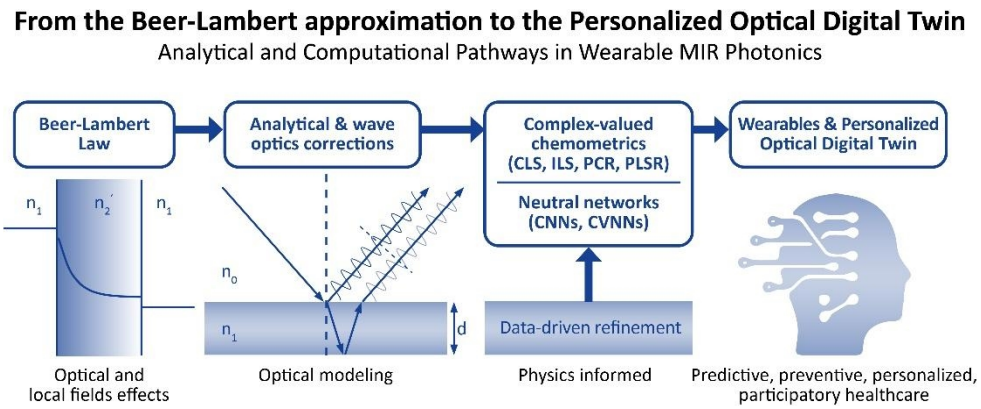

Fig. 5. From the Beer–Lambert law to the optical twin: Analytical and Computational Pathways in Wearable MIR Photonics. The schematic summarizes how deviations from the Beer–Lambert law (for instance, interference, ATR effects, local-field interactions, mixture non-idealities, biological scattering) motivate progressively more advanced analytical strategies—from classical chemometrics to complex-valued regression and physics-informed neural networks—ultimately enabling reliable MIR wearable operation.

ATR may also couple with interference, producing even stronger deviations from the BBL approximation.

3.1.3. Local-field effects

Molecules in condensed phases interact with the near fields of their neighbors, shifting resonance frequencies and modifying oscillator strengths. Planck described such deviations more than a century ago [93], and they remain evident in concentrated solutions where C = O vibrational bands shift inconsistently with linear scaling. These effects are approximately described by the Lorentz–Lorenz relation, which contains Beer's law as a limiting case for weak oscillators [91,92].

3.1.4. Non-ideal mixtures

Even thermodynamically ideal binary mixtures defy linear additivity. Principal component analysis of benzene–toluene or acetone–chloroform spectra reveals more than two components, while two-dimensional correlation spectroscopy exposes asynchronous features indicative of solvatochromism and environment-dependent polarizabilities [104]. Mixture spectra therefore cannot be reconstructed as simple linear combinations of their pure components.

3.1.5. Complex biological matrices

Scattering from cells, anisotropy from lipids and proteins, and wavelength-dependent path lengths from hydration collectively invalidate linear models. Water dominates large regions of the MIR spectrum, overlapping with weaker biomarker bands. In such matrices, deviations from the BBL approximation are the rule rather than the exception.

Mitigating these effects requires a two-pronged strategy. Some deviations can be addressed analytically. Fresnel-based multilayer models can reconstruct dielectric functions from interference-dominated spectra [88]. For ATR, rigorous wave-optics corrections that account for incidence angle, polarization, and refractive index contrast—often combined with Kramers–Kronig analysis—allow geometry-independent evaluation [88]. Once geometry and optical constants are known, these methods require no empirical calibration.

Optical Materials EXPRESS

Other deviations, particularly those from local-field interactions and non-ideal mixtures, resist analytical solutions. Here, chemometric methods provide the most effective remedy.

3.2. Classical chemometrics: CLS, ILS, PCR, and PLSR

The limitations of the Beer–Lambert approximation, particularly in wearable and biological contexts, demand more advanced regression strategies. A major step forward is the transition from real-valued to complex-valued chemometrics, where both the absorption index (k) and refractive index (n) are analyzed together. These quantities are linked by the Kramers–Kronig relations, meaning that every absorptive feature in k is accompanied by a corresponding dispersive response in n. Conventional chemometrics, based solely on absorbance, ignores this complementary information. By exploiting the full complex refractive index, regression models gain not only accuracy but also internal consistency checks and error-detection capabilities.

Classical Least Squares (CLS) remains one of the most transparent approaches in quantitative spectroscopy [105–107]. It assumes that a mixture spectrum is a linear combination of pure component spectra, each weighted by concentration. When extended to complex-valued spectra, CLS yields complex concentration estimates whose real parts represent physical concentrations, while the imaginary components capture systematic deviations from linearity [108]. These deviations reflect local-field interactions or wave-optical effects and can be used for internal correction: correlations between the imaginary part and prediction errors allow mean absolute errors to be reduced substantially. Case studies on benzene–toluene and benzene–cyclohexane mixtures show error reductions of up to 75% compared to conventional CLS, demonstrating how the dispersive dimension sharpens quantitative analysis [108].

Inverse Least Squares (ILS) addresses one key limitation of CLS—the requirement for pure component spectra—by inverting the relationship between spectra and concentrations [105–107]. This enables calibration even when not all mixture components are known. Traditional ILS, however, often suffers from ill-conditioning when applied across entire spectra. Incorporating refractive index information mitigates this instability: complex-valued ILS smooths spectral variability and integrates concentration-dependent dispersion, producing more stable regressions. In benzene–toluene systems, complex ILS reduced prediction errors by more than half relative to classical CLS and ILS, and in some cases by an order of magnitude [109].

Principal Component Regression (PCR) combines dimensionality reduction with regression, projecting spectra into a low-dimensional subspace defined by principal components before correlating them with concentrations [105–107]. The complex extension of PCR adds flexibility by generating eigenvectors either from complex singular value decomposition (SVD) or by pairing the eigenvectors of the imaginary part with their Kramers–Kronig transforms [110]. The latter creates superpositions that better represent the coupled absorption–dispersion behavior of real spectra. Studies on binary mixtures confirm that complex PCR generally outperforms conventional PCR in both predictive accuracy and robustness, though eigenvector selection in the complex plane remains an open question.

Partial Least Squares Regression (PLSR) is the most widely applied regression method in spectroscopy because it maximizes covariance between spectral data and concentration profiles [105–107]. Complex-valued PLSR extends this principle by including both n and k spectra, thereby accounting for dispersion as well as absorption [111]. Several implementations exist: (i) NIPALS algorithms that process real and imaginary parts separately, (ii) brute-force superpositions of real and imaginary eigenvectors optimized through cross-validation, and (iii) direct SVD of the complex cross-product matrix. Brute-force approaches ensure unbiased component selection, while SVD provides a computationally elegant alternative. In systems where refractive index variations dominate at high wavenumbers, complex PLSR achieves prediction errors an order of magnitude smaller than conventional PLSR based on the absorption index function alone.

Optical Materials EXPRESS

Collectively, these methods establish complex-valued chemometrics as a unifying framework for quantitative spectroscopy. Each approach exploits the absorption–dispersion interplay differently: CLS offers transparency and internal error correction; ILS provides calibration without pure spectra and enhanced stability; PCR improves robustness through complex eigenvector combinations; and PLSR delivers exceptional predictive power in challenging systems. A shared advantage is their ability to quantify deviations from the Beer–Lambert law instead of treating them as random noise—an essential feature for wearable spectroscopy, where such deviations are inevitable.

Finally, when refractive index data are unavailable, the same complex-valued framework can be applied to absorbance spectra alone. Although this sacrifices some accuracy due to missing dispersive information, the imaginary component of the regression output can still serve as an internal indicator of model reliability, providing valuable error estimates and maintaining a degree of robustness.

3.3. Convolutional neural networks in infrared spectroscopy

The transition from classical and complex-valued chemometrics to machine learning mirrors the growing complexity of data generated by wearable and flexible infrared devices. While regression methods such as CLS, ILS, PCR, and PLSR can accommodate many deviations from the Beer–Lambert approximation, they remain fundamentally linear. Biological tissues, heterogeneous mixtures, and flexible architectures introduce nonlinearities that may resist such frameworks. In these cases, deep learning—particularly convolutional neural networks (CNNs)—offers a more adaptive, end-to-end alternative.

Originally developed for image analysis, CNNs are well suited for infrared spectroscopy, where spectra can be treated as one-dimensional signals. Convolutional filters extract local spectral features such as characteristic band shapes, correlations between adjacent wavenumbers, and distortions caused by scattering or mixture effects. Unlike classical chemometrics, CNNs require no handcrafted pre-processing, as they learn directly from raw data.

One of their earliest and most compelling uses lies in artefact correction. Scattering—especially Mie scattering from cells or particles—has long limited quantitative analysis. Physically based corrections demand detailed optical modeling and are often restricted to ideal geometries. CNNs can instead learn these transformations empirically. Guo et al. trained a one-dimensional U-Net on synthetic PMMA sphere spectra generated via Mie theory, showing that the network could restore distorted spectra and compensate for resonant sphere modes without explicit optical parameters [112]. Similar autoencoder networks successfully mimicked RMieS correction, even outperforming it in robustness [113]. Such approaches demonstrate how CNNs can replicate complex physical models in real time, an important step toward automated correction within wearable systems.

Beyond pre-processing, CNNs excel in classification and regression. Chen et al. used a one-dimensional CNN to distinguish aristolochic acids and analogues with higher accuracy than support vector machines or conventional chemometrics [114]. Zhang *et al.* extended this to two-dimensional CNNs for classifying tobacco leaf origins, where CNNs surpassed PLS-DA in accuracy and robustness [115]. CNNs can also perform quantitative regression, learning nonlinear mappings between spectral features and concentrations and thus outperforming PLSR or PCR, particularly for overlapping or distorted spectra. Their resilience to background absorption and scattering makes them well suited for wearable applications.

The strengths of CNNs lie in automated feature extraction, nonlinear modeling, and scalability with dataset size [113]. However, they require large, diverse datasets to generalize reliably. Their "black-box" nature limits interpretability, and while they can reproduce physical corrections, they do not inherently provide mechanistic insight. These limitations motivate hybrid approaches such

Optical Materials EXPRESS

as physics-informed neural networks (PINNs), which embed constraints from Fresnel relations etc. or Kramers–Kronig consistency into the learning process [116,117].

Unlike conventional CNNs, complex-valued neural networks (CVNNs) operate directly on complex quantities such as electromagnetic fields or refractive indices, allowing them to capture absorption and dispersion simultaneously. This integration of optical physics with deep learning could yield interpretable, causal models ideal for real-time correction and diagnosis in future infrared wearables.

3.4. Infrared wearables within the personalized optical digital twin

The evolution from the Beer–Lambert law through complex-valued chemometrics to physics-informed complex-valued neural networks marks a continuous broadening of spectroscopy—from simple analytical laws to adaptive learning systems. Yet these methodological advances achieve their full impact only when embedded in devices capable of continuous, non-invasive health monitoring. Within this framework, infrared wearables have emerged as cornerstone technologies of the Personalized Optical Digital Twin (PODT).

The PODT is envisioned as a continuously updated, light-based digital representation of an individual's health, designed to detect risks and deviations before symptoms appear and a pictorial representation is given in Fig. 6. It integrates multiple information layers: physiological signals such as heart rate and oxygenation, structural imaging from modalities like OCT, and molecular fingerprints of metabolites, proteins, and lipids. Among these, IR spectroscopy uniquely provides the molecular layer, directly probing vibrational modes in the fingerprint region to yield specific biochemical signatures.

Fig. 6. Schematic representation of the Personalized Optical Digital Twin (PODT) concept as envisioned by Photonics21. The diagram illustrates the integration of physiological, structural, and molecular optical data—including MIR spectral biomarkers—into a continuously updated digital model of individual health, used to enable early risk detection and predictive, personalized interventions.

Wearable mid-infrared devices—implemented as skin patches, microneedle platforms, or textile-integrated sensors—can generate continuous spectral streams reflecting an individual's biochemical dynamics. Sampling sweat, interstitial fluid, or breath condensates, such sensors enable high-frequency molecular monitoring. Subtle metabolic fluctuations preceding diabetes, or spectral markers associated with early tumorigenesis, could thus be detected long before

Optical Materials EXPRESS

conventional diagnostics. Flexible IR badges may also track environmental toxin exposure, linking external stressors directly to personal health trajectories.

Achieving this vision demands major technical progress. The light–tissue interface must remain stable despite motion, hydration changes, and skin variability. MIR sources and detectors must be miniaturized, power-efficient, and fabricated on flexible substrates without loss of sensitivity. Long-term, unsupervised operation requires embedded intelligence to manage drift, noise, and artefacts. Here, complex-valued chemometrics and physics-informed complex neural networks can serve as on-board analytical engines—stabilizing spectra, performing plausibility checks, and estimating concentrations in real time.

Equally important are regulatory and societal factors. For PODTs to gain clinical acceptance, they must comply with medical device regulations, ensure cybersecurity, and provide transparent audit trails for AI-driven decisions. Clinicians need interpretable outputs rather than raw spectra, while patients must trust that their molecular data are securely managed and clinically meaningful. Building this trust depends as much on governance, interoperability, and long-term maintainability as on photonic innovation.

Infrared wearables are therefore not auxiliary tools but fundamental enablers of the PODT. They supply the biochemical data layer that anchors digital twins in molecular reality, ensuring that predictions reflect true physiological processes rather than abstract models. In combination with Raman spectroscopy, OCT, fluorescence imaging etc., and complementary biosensors, MIR wearables will provide a holistic view of health.

As healthcare systems confront chronic disease, aging populations, and the need for resilience against pandemics, the potential of infrared wearables becomes unmistakable. By continuously monitoring molecular fingerprints at the body's surface, they transform the PODT from a digital mirror into a proactive guardian—detecting subtle biochemical changes before symptoms arise and guiding timely intervention. The trajectory from Bouguer-Beer-Lambert's exponential law to the optical digital twin thus comes full circle: what began as a study of light attenuation now illuminates a future where light itself safeguards human health.

Realizing these analytical and computational concepts in practice requires light sources capable of delivering spectrally selective, high-power mid-infrared radiation within compact and manufacturable architectures—a challenge addressed in the following section through hybrid III–V/silicon Quantum Cascade Lasers.

4. From hybrid III–V/silicon quantum cascade lasers for integrated mid-infrared photonics

4.1. Hybrid III–V/silicon quantum cascade lasers

The analytical and computational advances outlined in Section 3 define quantitative and algorithmic requirements that directly influence the design of MIR light sources. Accurate complex-valued chemometric and neural-network analysis relies on stable, spectrally pure, and intensity-calibrated illumination at well-defined wavelengths. In wearable configurations, the optical power must remain high enough to overcome scattering and interference losses while avoiding thermal or phototoxic effects.

These criteria naturally guide the hardware concept toward *spectrally agile, multi-wavelength, and power-efficient* sources—capabilities that are uniquely offered by Quantum Cascade Lasers (QCLs). Moreover, algorithmic models exploiting Kramers–Kronig-consistent dispersion data or multi-spectral CNN inputs benefit from the ability to tune the emission wavelength precisely across molecular resonances. Consequently, the integration of QCL arrays within CMOS-compatible platforms provides the technological foundation for implementing the spectral modeling framework in practical, miniaturized devices.

As discussed in previous sections there is a strong need for efficient low-cost devices which could monitor biomarkers using several marker wavelengths. With this regard we believe that the

Optical Materials EXPRESS

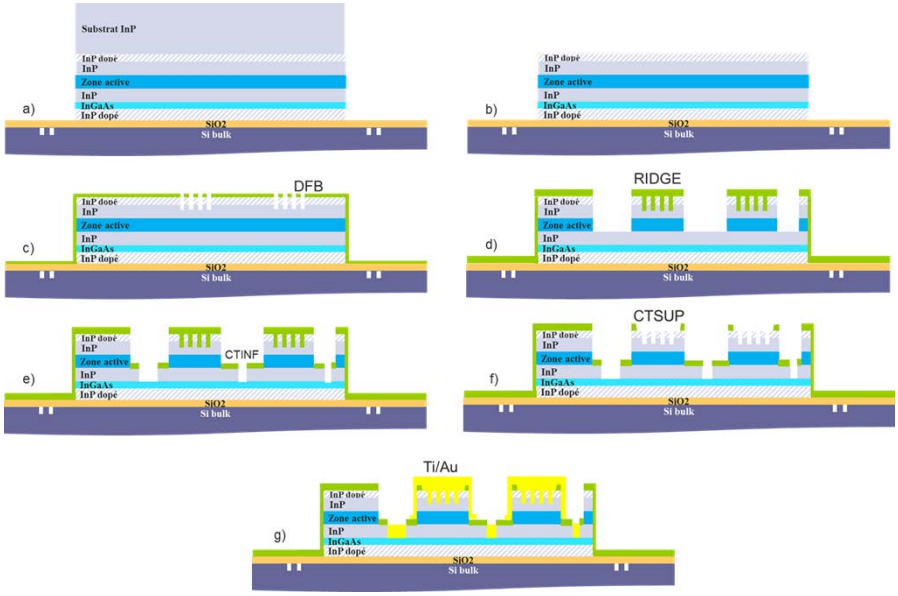

Fig. 7. Process flow for the fabrication of a QCL device transferred onto silicon: (a) molecular bonding of the III–V epitaxial stack onto Si, (b) removal of the native substrate, (c) DFB grating etching, (d) ridge definition, and (f–g) successive metallization steps.

integration of quantum cascade lasers (QCLs) with silicon-based photonic circuits represents a decisive milestone for mid-infrared (MIR) optoelectronics. In particular we address the issue of integrating an array of laser sources to probe the samples at multirole wavelengths. As discussed in previous sections the MIR spectral range most interesting part, extending from roughly 3 µm to 12 µm, encompasses the fundamental vibrational resonances of most molecules, making it an essential domain for applications such as gas sensing, environmental monitoring, chemical spectroscopy, and biomedical diagnostics. Despite their maturity and spectral agility, QCLs fabricated on InP or GaAs substrates remain limited by small wafer diameters, high fabrication costs, and poor compatibility with large-scale CMOS manufacturing. Bridging QCL technology with silicon is therefore a strategic step toward scalable, cost-effective, and industrially viable MIR systems [118].

Hybrid III–V/silicon integration provides the technological foundation for this transition, combining the spectral reach and gain of III–V semiconductors with the precision, yield, and process maturity of silicon photonics. This approach aims to establish a wafer-level platform where active sources, passive routing structures, and detectors coexist within a unified fabrication ecosystem. Achieving this requires mastering three essential aspects: a thermally and optically robust bonding interface, efficient optical mode transfer between dissimilar materials, and a photonic design that guarantees single-mode operation and power efficiency across large wafers [39,118].

A first level of integration establishes a mechanically and thermally stable III–V/Si platform in which the entire laser cavity remains confined within the III–V epitaxial material, while the silicon substrate serves as a passive mechanical and thermal carrier. The complete fabrication process is illustrated in Fig. 7, summarizing the plasma-activated molecular bonding process, substrate removal, DUV lithography for defining the DFB gratings and ridge, and the final metallization sequence. This CMOS-compatible process, as demonstrated in a 200 mm CMOS pilot line [39], enables the transfer of III–V epitaxial layers onto silicon with excellent planarity

Optical Materials EXPRESS

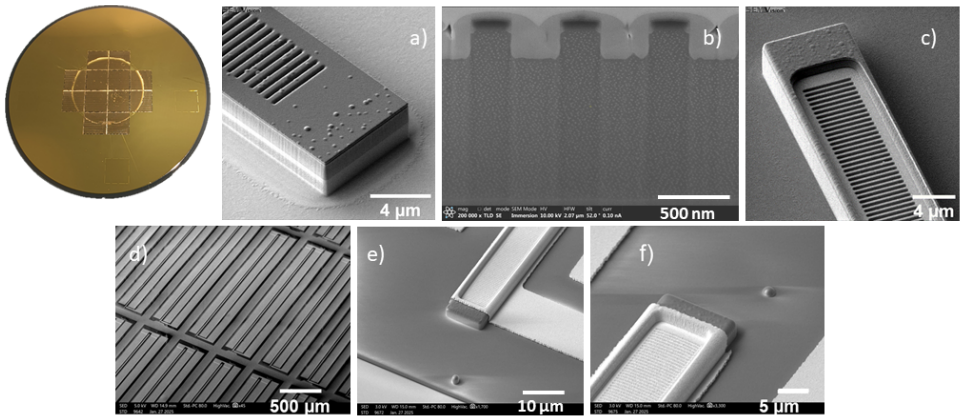

Fig. 8. Scanning electron microscopy (SEM) images acquired at successive fabrication stages: top view of the DFB ridge (a), cross-section of the DFB grating (b), hard-mask opening prior to metallization (c), and completed QCL devices after metallization (d–f).

and interface quality. The oxide-bonded route provides high interfacial reliability and uniformity across the wafer, ensuring reproducibility and surface integrity. In parallel, a titanium-mediated bonding variant is being developed to improve thermal conduction and electrical injections across the interface, providing a complementary route for heat management.

Representative structural results for oxide-bonded devices are presented in Fig. 8. Scanning electron and optical microscopy images reveal the accuracy of the DFB ridge definition, the smoothness of the etched gratings, and the uniformity of the metallization layers across the wafer. These results confirm the maturity of the lithographic and etching processes, as well as the robustness of the molecular bonding interface. Such integration enables high-yield fabrication of III–V/Si quantum cascade lasers directly on 200 mm silicon wafers, a decisive step toward large-scale production.

Electrical and optical characterizations at wafer level are summarized in Fig. 9. Under pulsed excitation, oxide-bonded devices exhibit threshold currents around 0.8 A for emission near 4.05 µm, consistent with the design of the distributed feedback gratings. The emission spectra show single longitudinal mode operation, with well-defined peaks and limited parasitic modes, attesting to the spectral purity of both individual DFB structures and QCL-DFB arrays. These measurements are performed directly on-wafer, prior to any packaging, demonstrating the robustness of the oxide-bonded architecture and its potential for industrial testing. The titanium-bonded configuration, although still under optimization, has recently shown quasi-continuous-wave operation at wafer level (duty cycle $\approx 40\%$) and a more than 100-fold increase in average optical power compared to the oxide-bonded baseline. These results underline the crucial role of thermal management in hybrid QCL operation and open the path toward true continuous-wave emission.

Building on this structural foundation, the silicon layer can evolve from a passive carrier to an active photonic participant. In the functional hybrid configuration (see Fig. 10), the III–V gain region is optically coupled to a phase-matched silicon-on-nitride-on-insulator (SONOI) waveguide that implements distributed feedback and efficient out-coupling. The adiabatic coupling along a ~290 µm taper ensures gradual mode transfer between III–V and silicon with minimal reflection and power loss. The calculated coupling strength provided by the silicon DFB grating ensures single-mode operation with low optical losses and excellent modal confinement within the hybrid cavity [19]. Finally, surface grating couplers enable direct wafer-level optical access, facilitating collective electro-optical characterization.

Optical Materials EXPRESS

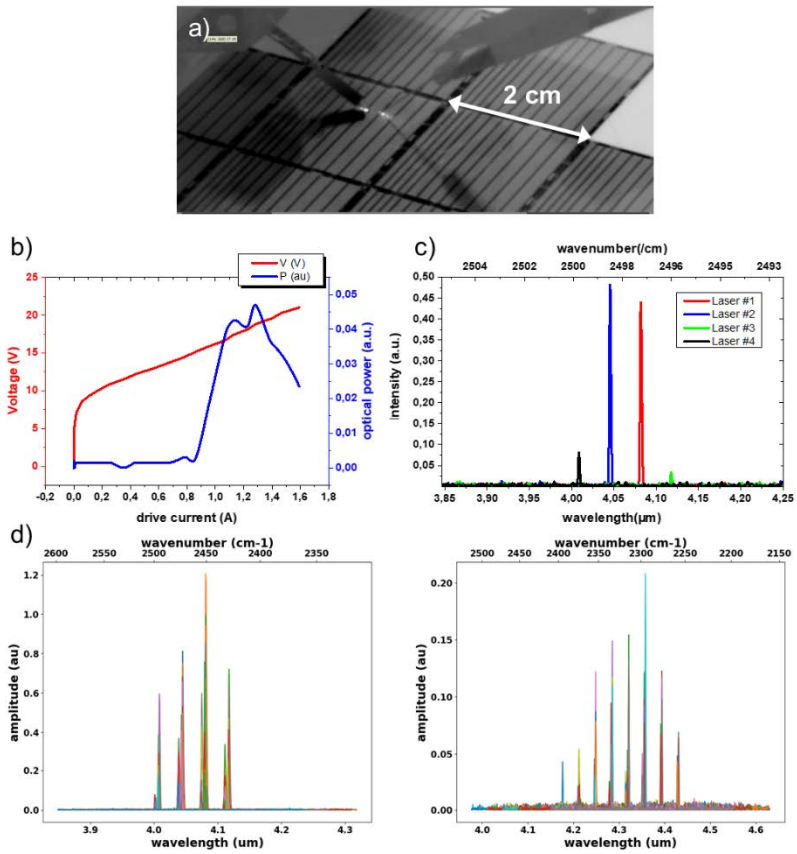

Fig. 9. Wafer-level electro-optical performance of oxide-bonded QCLs. Infrared imaging reveals uniform device operation across the wafer (a), while current–voltage–light (IVL) measurements confirm lasing at 4.05 µm with well-defined thresholds (b). Characterization of QCL bars incorporating different opto-geometrical configurations (c–d) demonstrates the design flexibility and process reproducibility of the oxide-bonded platform (each color corresponds to a single-mode laser emitting at a distinct wavelength).

The experimental validation of this functional approach is illustrated in Fig. 11. Light–current–voltage measurements demonstrate a threshold current density of approximately 3.5 kA·cm^{-2} at 12 °C, with a driving voltage around 16 V. The output optical power reaches 340 µW per facet (around 500 µW on-chip) when measured through the silicon surface coupler. The emission spectra are centered at 4.315 µm with a side-mode suppression ratio exceeding 25 dB, confirming robust single-mode operation. These performances, reproducible across the wafer, demonstrate that hybrid III–V/Si devices could equal the performance of conventional InP-based QCLs while benefiting from the scalability and integration potential of silicon photonics [19,119].

The convergence of these two integration routes—structural and functional—defines a coherent technological framework for MIR photonics. The oxide-bonded platform provides high yield, reproducibility, and interface quality, while the titanium-bonded variant introduces improved heat spreading and enhanced current injection for near-continuous operation. The SONOI-based functional integration extends this foundation by enabling photonic routing, spectral control, and wafer-level optical access within a unified architecture. Together, these technologies pave the way for compact, efficient, and scalable MIR laser sources monolithically compatible with large-volume silicon photonic manufacturing.

Optical Materials EXPRESS

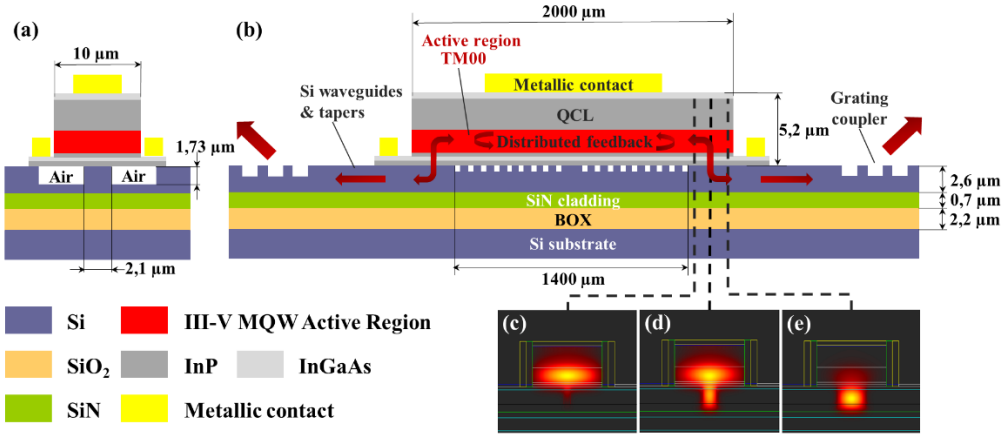

Fig. 10. Functional hybrid integration on a phase-matched SONOI platform. Transverse (a) and longitudinal (b) schematic views of the hybrid laser cavity show that the optical mode is predominantly confined within the III–V active region while interacting with the underlying silicon grating, which provides distributed feedback for single-mode operation. At each end of the active region, a silicon taper ensures an adiabatic transfer of optical power from the III–V section to the silicon waveguide. Grating couplers positioned at both ends of the laser extract the emitted light from the chip for collection by an optical fiber. (c–e) Simulated evolution of the fundamental TM_{00} optical mode along the taper: (c) taper input, (d) taper midpoint, and (e) taper output, highlighting smooth modal transition and high coupling efficiency. Reprinted with permission from Ref. [19].

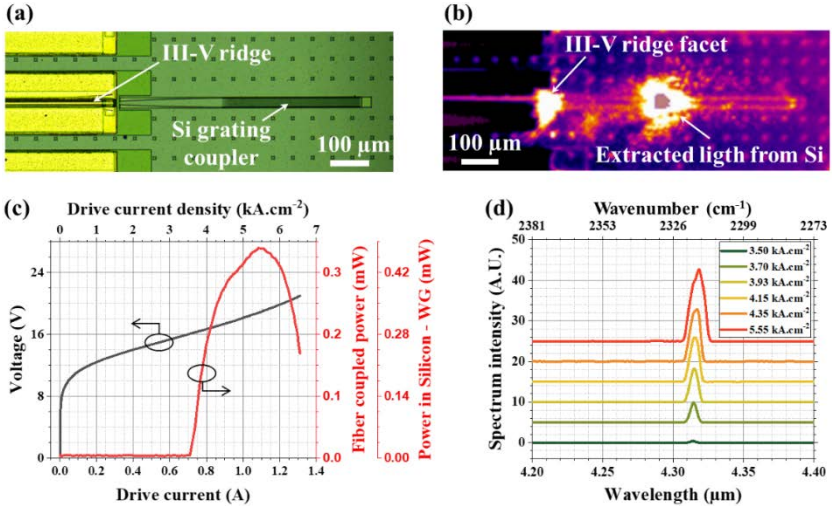

Fig. 11. Experimental validation of the functional hybrid III–V/Si QCL architecture.(a) Visible and (b) infrared microscope images of the laser under pulsed operation at peak output power. Light generated within the III–V active region is adiabatically coupled into the silicon waveguide and extracted through a 350 µm-long surface grating coupler. (c) Single-facet light–current–voltage (LIV) characteristics measured at 12 °C (300 ns pulses, 0.6% duty cycle). (d) Corresponding emission spectra as a function of injection current density, confirming stable single-mode operation and efficient optical coupling through the silicon grating. From Ref. [19].

Optical Materials EXPRESS

From a manufacturing perspective, all the approaches described rely on CMOS-compatible processes encompassing bonding, lithography, metallization, and wafer-level testing. The reproducibility achieved across 200 mm wafers establishes a realistic path toward industrial fabrication of MIR sources and their integration into complete on-chip systems for spectroscopy, free-space communication, and sensing. Ongoing work focuses on quantitative thermal modeling of Ti-assisted bonding, time-resolved thermos-reflectance measurements, and packaging optimization to achieve continuous-wave operation at room temperature.

Beyond these technological advances, hybrid III–V/silicon integration unites materials science, photonic engineering, and industrial processing into a single scalable platform. By combining the reliability of oxide bonding, the thermal efficiency of metallic interfaces, and the optical sophistication of silicon photonics, this technology enables high-performance, manufacturable MIR lasers at wafer scale. The experimental results summarized in Fig. 7–11 establish a continuum from material transfer and process optimization to photonic integration and system-level validation, marking a decisive step toward fully integrated mid-infrared photonic systems combining on-chip sources, routing, and detection.

The modeling approaches developed in Section 3 place quantitative demands on the light-source architecture. Accurate chemometric calibration requires sub-cm^{-1} spectral reproducibility, while physics-informed neural networks benefit from tunable, multi-wavelength input to resolve correlated absorption–dispersion features. Furthermore, real-time data pipelines impose constraints on source modulation bandwidth, duty cycle, and thermal stability. These considerations inform the choice of QCL arrays as the enabling hardware for the envisioned wearable MIR systems.

4.2. Application to QCL and photo-acoustic measurements

Photoacoustic (PA) spectroscopy relies on the localized heat release within a gas sample following the absorption of modulated light energy. When a gas absorbs light at specific wavelengths—characteristic of its molecular composition—non-radiative relaxation processes, primarily through molecular collisions, convert the absorbed optical energy into heat. This localized heating induces transient thermal expansion and contraction, generating both thermal and acoustic waves.

The acoustic wave is produced as a result of the periodic modulation of the incident light intensity or wavelength, typically at a frequency matching the acoustic resonance of the PA cell, often in the kilohertz range. The resulting pressure fluctuations are then detected as an acoustic signal by a sensitive microphone housed within the PA cell. The light source may be either a pulsed laser or a continuous-wave light beam, with the modulation frequency selected to optimize the acoustic response of the cell.

This approach enables highly sensitive and selective gas detection, as the PA signal is directly proportional to the absorbed optical energy and, consequently, to the concentration of the target gas species [120,121].

4.2.1. Photoacoustic positioning versus direct absorption detectors

During the direct absorption of light through a gas sample, the incident optical power P_0 is attenuated according to the Beer–Lambert law as follows:

$$P = P_0 e^{-\alpha C_g L} \tag{2}$$

While Eq. (1) expresses the Bouguer–Beer–Lambert relation in its analytical-chemistry form - using absorbance as a linear function of molar absorptivity, concentration, and path length - the same principle can also be written in terms of the transmitted optical power. In this representation (Eq. (2)), the exponential attenuation of the incident power P_0 is described through the absorption coefficient $a(C_g)$, which implicitly includes both molecular absorption properties and concentration. This formulation assumes a homogeneous medium and a collimated beam

Optical Materials EXPRESS

without divergence or scattering losses, so that the decrease in power directly reflects pure absorption along the optical path.

The photoacoustic signal is derived from the Beer-Lambert's law applied to the Helmholtz resonator according to the expression [122]:

$$S_{PA} = R_c R_M P \alpha C_g \tag{3}$$

Where the quantity R_C is

$$R_c = \frac{(\gamma - 1)LQ}{\omega_0 \, V_c} \tag{4}$$

And the definition of ω_0 and Q are

$$\omega_0 = \sqrt{\frac{S{c_g}^2}{lV_c}}, Q = 2\pi\sqrt{V_c\left(\frac{l}{S}\right)^3}, \tag{5}$$

Where R_M is the microphone constant R_c is the acoustic cell constant, g is the ratio of the specific heats of the gas, L the length of the photoacoustic cell, Q quality factor of the resonator, V_c the critical volume of the PA cell which is $V_c = (1/V_1 + 1/V_2)^{-1}$ for our differential Helmholtz resonator (DHR), S is the neck (capillary) section, l the length of neck, c the celerity of sound, Fig. 12.

Fig. 12. Helmholtz resonator schematic. Left: Main quantities important for the design and optimization of the differential Helmholtz resonator photoacoustic cell; Middle: PA cell fabricated in CEA-Leti clean rooms in Silicon (left part with a microphone on top and opened on the right side); Right: Schematic of the gas response in the two arms (opposite phase) and view of a PA cell with connecting gas input and output.

While the direct absorption technique requires a large optical path length L, to maximize the measurable attenuation of light, the photoacoustic (PA) method yields a signal amplitude inversely proportional to the chamber volume [123]. This property makes PA particularly advantageous for miniaturized designs and compatible with microfabrication-based manufacturing.

4.2.2. Concept and dimension of differential Helmholtz photoacoustic

The DHR consists of two identical chambers linked by two capillaries, with gas inlet and outlet at their midpoint. A laser excites one chamber, generating out-of-phase acoustic waves at the Helmholtz resonance frequency in both chambers. Two microphones measure the chamber pressures, and their differential signal provides a partial immunity to external acoustic noise. As the PA sensor does not require an optical detector but a sound detector it is not sensitive.

Several generations of DHR have been fabricated in our laboratory at CEA-LETI, with the same architecture [123,124]. Initially using 3D printing (metal or polymethylmethacrylate), as proof of concept, with a V_c of approximatively 40mm^3, and resonant frequency of 3kHz embedding a pair of commercial top port microphone glued on the metal block. A second

Optical Materials EXPRESS

generation of DHR has been produced from two silicon wafers patterned, etched, and bonded by the means of techniques commonly used in

MEMS foundries. The size and the critical dimensions have been adjusted in order to fit with the angular divergence and the location of the laser source coupled to the cell without optical lenses while having a resonance frequency in the range of 10 to 15kHz (Vc ~2.3mm^3). Metal contacts are patterned on the upper wafer in order to weld and connect the microphones and extract the electricals signal. After dicing the PA cells, two analogical AKU350 MEMS microphones are welded and the electrical contacts are wire-bonded to an electronic interface made with a printed circuit board (PCB) allowing the analogical signal processing. This namely miniPA-Si design reaches a chip size of 10×8 mm^2 with a thickness of few millimeters because of the commercial microphones added on top.

Reducing the volume of the PA chambers increases the resonance frequency and the influence of the viscous and thermal surface losses. So that miniaturization reaches fundamental limits. To ensure effective photoacoustic signal generation, the laser modulation frequency must remain sufficiently low (typically ≤ 20 kHz) to allow thermal relaxation of gas molecules and the resulting pressure fluctuations. This requirement is critical because relaxation times vary significantly depending on the target molecule and gas matrix. Setting an upper frequency limit ensures the photoacoustic (PA) cell design remains compatible with detecting multiple gas species. A third generation of DHR device have been developed including its own dynamic pressure sensor, designed to be fully integrated to the PA cell microfabrication and to provide a mechanical resonance less sensitive to environmental conditions (pressure, temperature, gas matrix. . .) than the acoustic resonance, Fig. 13, left and center.

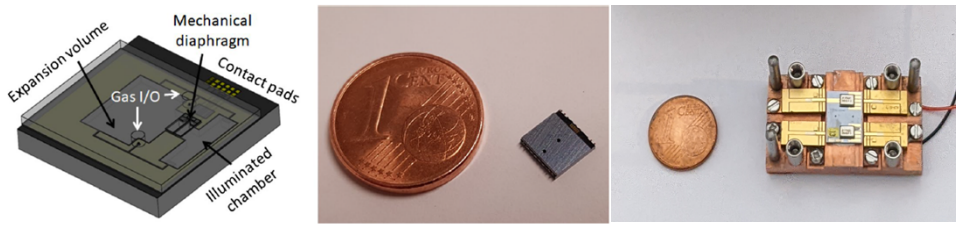

Fig. 13. 3D view of the silicon-integrated photoacoustic sensor (left),view of the manufactured chip (center), and view of the photoacoustic multi-gas sensors, with four QCL coupled with one silicon PA-cells (right)

4.2.3. Multi-laser coupling for multi-gas measurements

For multi-gas detection, several lasers tuned to the characteristic wavelength of the molecules must be coupled to the PA cell. The mini-PA Si, with its four optical windows, allows direct coupling of four different lasers targeting at least one gas per laser. Figure 13 right shows the multi-gas sensor mechanical assembly with four Quantum Cascade Laser (QCL) coupled with one Silicon Mini-PA. The mechanical parts are designed to enable self-aligning assembly of the lasers on the PA cell windows, with an accuracy of ± 50 µm, and the possibility of replacing each laser unit in the event of failure. The copper base that connects all the components is soldered to the rear to a Peltier element to ensure the thermoregulation of the lasers, Fig. 13, right.

The multigas measurement can be performed sequentially by activating the lasers one by one for a few hundred milliseconds to a few seconds for each gas.

Optical Materials EXPRESS

4.2.4. System approach, transducer (microphone), laser power supply and modulation, synchronous detection

In order to perform measurements using a portable, autonomous multi-gas sensor, we have developed a specific, compact electronic system dedicated to outdoor photoacoustic data acquisition. The independent components are the sensor power supply, multiplexing and QCL control (in pulsed or continuous mode), temperature control, microphone data collection, amplification, and signal processing. The entire system comprises several printed circuit boards (PCBs) for each block, which facilitates modifications and repairs. The size of the electronics remains large, typically 15 cm x 10 cm x 5 cm in its alpha version (see Fig. 14). Later, it could be reduced to a few tens of cubic centimeters with stacked PCBs, and then to a few cubic millimeters with integrated ASICS-type electronics.

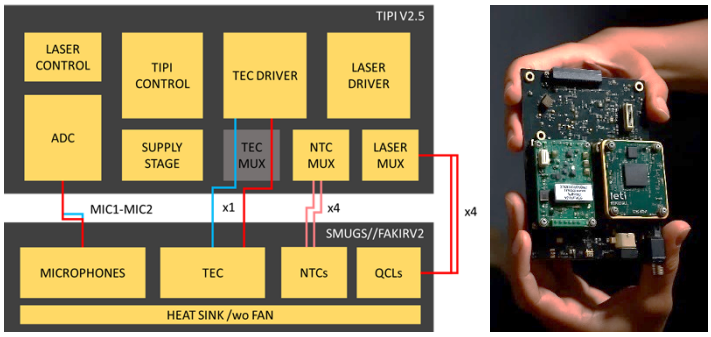

Fig. 14. Left: Functional diagram of the control electronics for a multigas photoacoustic sensor. Right: Photograph of the corresponding LETI electronic system (credit A. Aubert).

4.2.5. Gas/N2 and gas/air + Hr calibration results

An initial calibration step was performed for four target gases: CO_2, CH_4, N_2O, and CO, as shown in Fig. 15, using four different QCL delivering optical frequency tuned to match the absorption peaks of CO_2 (2361.4cm^{-1}), CO (2190.0cm^{-1}), CH_4(1341.6cm^{-1}), N_2O(2192.5cm^{-1}). Dilution conditions were established using high-purity nitrogen as diluent and standard gas cylinders calibrated to few hundred parts per million (ppm) for each gas. For all gases, the laser temperatures were regulated to 35°C, and photoacoustic signals were demodulated at 2F using a sinusoidal modulation frequency set to half the resonance frequency of the photoacoustic cell ($f_0/2 = 5000$ Hz) with an amplitude of few percent of the nominal laser power.

While calibrations under nitrogen do not replicate real-world atmospheric conditions—particularly variable humidity—they enable laboratory sensor qualification and the determination of detection limits (LOD) using a simplified linear calibration model.

Despite consistent calibration conditions, including PA cell purging with N_2, no cell constant (R_c) could be established for direct sensor calibration (e.g., for atmospheric CO_2). Linear regressions revealed substantial variations in baseline signals, suggesting strong background noise dependencies. Prior studies have reported gas-gas coupling effects (e.g., CH_4 and CO_2 interactions with N_2, O_2, or H_2O), which may enhance or suppress photoacoustic signals [125,126]. This was further confirmed by calibrations performed in air (N_2+O_2+CO_2) with variable relative humidity (Hr), Fig. 16.

An enhancement of the PA signals by a factor of 5 for CO_2 in air was observed in samples with 60% of relative humidity compared to that in dry samples. Water provides a strong enhancement in the CO_2 molecular relaxation process increasing the slope of the calibration line as much as

Optical Materials EXPRESS

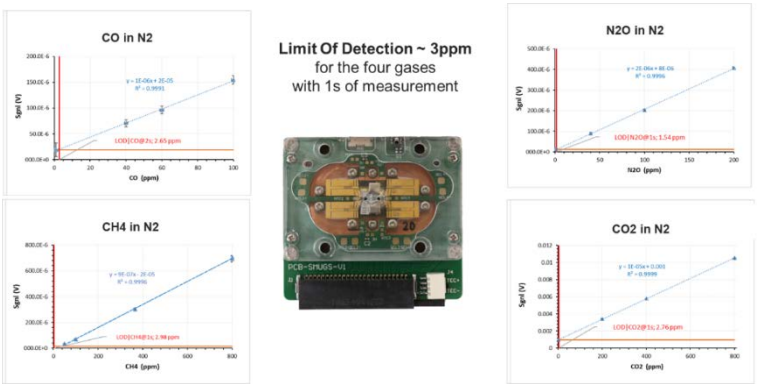

Fig. 15. Multigas calibration in nitrogen, for CO, N2O, CO2 and CH4 with a limit of detection of few parts per million (ppm). Center: view of the PA module including PA cell, 4 different QCL, connections, a copper base and a Peltier element at rear to ensure the thermoregulation of the lasers. Around: graphs showing the calibration result for different gases (CO, N_20, CH_4 and CO_2) diluted in N_2 matrix

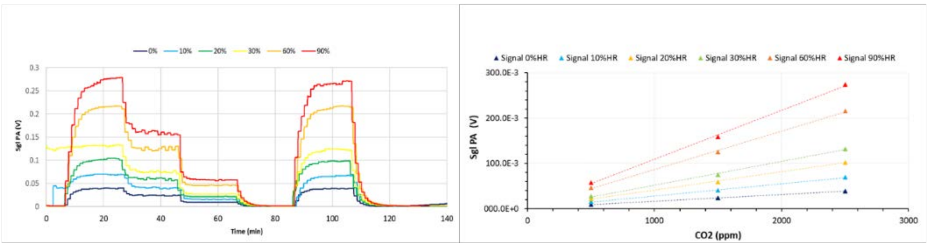

Fig. 16. Left: Photoacoustic signal for CO: 2500, 1500, 500 ppm with different humidity levels. Right: CO2 calibration lines for 0% to 90% of humidity.

the humidity is higher. The same type of behavior is observed for CO and N2O, while the PA signal for CH4 is less affected by humidity.

4.3. Towards non-invasive glucose monitoring with QCL-based MIR spectroscopy and photothermal transduction

Non-invasive glucose monitoring has been a relentless research topic for a few decades. It is pushed by the patients, who wish for less invasive and stigmatizing monitoring devices, and an alarming increase in diabetes prevalence [127,128]. Yet, no satisfactory solution has emerged, and the field is often regarded as a startup graveyard [129]. Indeed, without direct physical access to the glucose molecules (that for example a needle can provide), one has to deal with human physiology and anatomy complexity. Whatever the technical solution retained, its interpretation is not straightforward. In practice, it should be coupled with an acute biological knowledge of the probed region, and often, complementary measurements.

MIR spectroscopy is still in the game to compete in this race [130]. It benefits from better specificity than other electromagnetic spectral ranges [131], and the gain in maturity of quality MIR optical sources: QCLs. We shall return to those two aspects limitations below. The main MIR spectroscopy approach retained for embedded devices is photothermy. It consists of an indirect detection of the heat released by the optically probed sample [132,133]. Transmission spectroscopy is out, as the optical absorption length is typically a few tenths of micrometers, and

Optical Materials EXPRESS

ATR spectroscopy unfit since it only penetrates a few micrometers deep, where no glycemic signal can be found on the human skin.

Figure 17 shows a typical MIR photothermy experiments on human skin. The optical beam arrives perpendicularly to the skin, that is, at the scale of the beam diameter, approximated by a succession of vertical biological layers. The light is absorbed according to the Beer-Lambert law, which results in a heat source whose intensity decays with successive exponential trends, their steepness depending on the source wavelength and the layers' composition. There are multiple ways to detect heat release. The scientific literature is concentrated on two of them. The first consists of measuring the temperature fluctuation provoked by the heat released in a controlled media affixed to the sample. This medium can be regarded as a thermal transducer. For example, indirect photoacoustic uses a gas cavity to generate an acoustic wave [40,134–136] (see Fig. 17), and thermal deflection uses a solid with a refractive index sensitive to the temperature coupled with a probe beam [137]. The second detects the acoustic wave generated by the heat source induced sample dilatation [138], either in transmission or reflection.

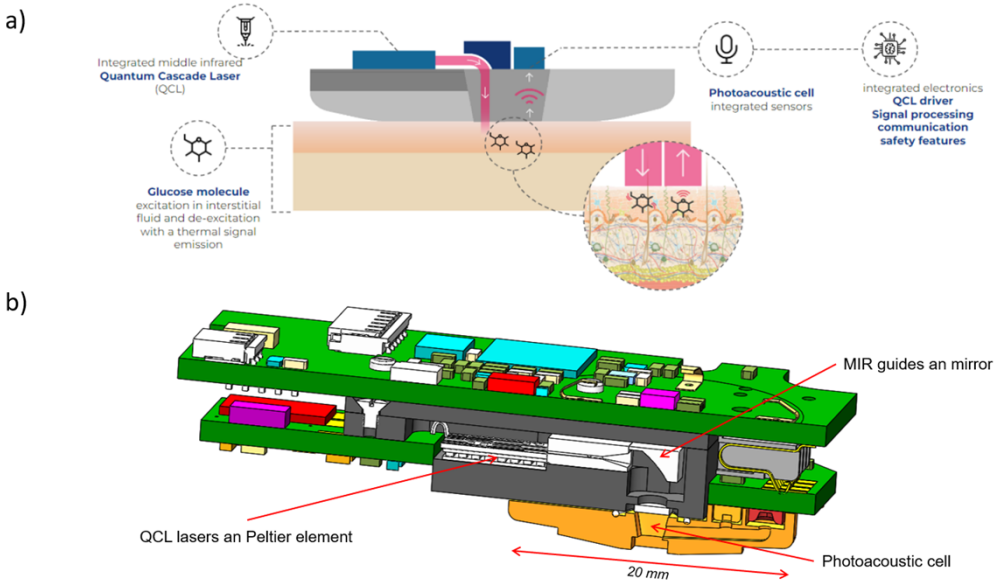

Fig. 17. a) Schematic diagram of a non-invasive glucose monitoring device with MIR spectroscopy and photothermal detection (the figure is detailed in [40]). The device is set on the skin, represented here as two homogeneous layers: at the top the stratum corneum, and at the bottom the epidermis in which glucose is contained inside the interstitial fluid. b) Example of a practical realization of the concept presented in a) (CAD cross-section view). This device is a version close to the one presented in Ref. [40].

While glucose has a specific MIR signature, it is hard to detect on human skin. First, glucose is mixed with other compounds whose signatures can be stronger (water, lactate), or of the same order of magnitude (urea, albumin, cholesterol, etc). Those interferents have their own temporal trend that is, or is not, correlated with the glycemic level. Second, the human skin, at the scale of the optical absorption length, is not homogeneous (see Fig. 17). MIR light typically penetrates down to 50 μm into the skin. It goes through the *stratum corneum*, where no glucose characteristic of the blood glycemic level can be found, and ends in the *epidermis*, where glucose is present inside the interstitial fluid. The layers' thickness and composition change with time, position on the patient, and from one patient to another. This variability induces a tremendous complexity for signal interpretation. To tackle this problem, technical solutions are multiplying

Optical Materials EXPRESS

the optical sources (in order to decorrelate the contributions from the various skin compounds) and developing strategies to retrieve spatial information (to separate the contributions from the different skin layers). Also mandatory is a precise understanding of how this complex environment acts as a whole. More precisely, how the skin structure and composition may have a response correlated to the blood glycemic level. By doing so, we can benefit not only from the glucose MIR specific signal, but also from the skin interferents signatures. A powerful way to integrate this knowledge for measurement understanding and interpretation is to pass through the development of a skin numerical twin [40,134].

Although QLCs are powerful and conveniently tunable optical sources, their opto-electrical efficiency is low (typically a few percent). Therefore, the main issues when developing a wearable system with QCLs are: how to deal with the device heat release, and how to manage its autonomy. The problems are addressed by seeking any opportunity to minimize the lasers' operating time (while keeping the necessary information for further interpretation) and integrating ingenious design strategies for heat dissipation (for example using the forearm as a heat sink). Incorporating QCLs in embedded medical devices raises other issues, that however remain easier to tackle than the heat issue: optical safety, the conception of MIR optics for beam management, the laser temperature fine control, and the development of miniaturized high voltage pulsers.

Up to date, [40] is the first and only wearable QCL device that went through clinical trials.

The device data streams derived from QCL-based wearables, in turn, provide the empirical foundation to refine and validate the complex-valued chemometric and neural-network models described in Section 3, completing the feedback loop between optical modeling and hardware development.

5. Conclusions

We discussed the importance of the Mid-infrared wavelength interval and in particular of the fingerprint wavelength interval for spectroscopy and application to the biomedical field. We are convinced that Mid-Infrared wearable and portable photonics devices will provide a giant leap in the chemical and biomedical analyses once cost-effectiveness and compactness/integration is achieved. We propose a pathway based on two research lines. The first is improved physical light propagation models, with Artificial Intelligence and Machine Learning post-processing. The second is to ensure low-cost mass production of arrays of Quantum Cascaded Lasers, using C-MOS technology, with integrated photoacoustic detection. This technology may offer a reliable approach for efficient devices in the very near future. A first glucose monitoring wearable devices, here presented, has already been through clinical trial. Wearable and portable Mid-infrared sensors will be important and necessary for supplying additional molecular fingerprint data and creating the overall biochemical foundation of the Personalized Optical Digital Twin. This will provide a dynamic representation of a person's molecular state to shift healthcare from reactive treatment toward predictive and preventive monitoring.

Funding. Politecnico di Torino (51_RIF20ST); Intesa Sanpaolo Innovation Center (51_RSG20ST); Thüringer Ministerium für Wirtschaft, Wissenschaft und Digitale Gesellschaft; Bundesministerium für Bildung und Forschung; Fonds der Chemischen Industrie; Carl-Zeiss-Stiftung; Horizon 2020 Framework Programme; French Public Authorities (France 2030 program).

Acknowledgments. Stefano Taccheo acknowledges support from the Starting Grant of Politecnico di Torino, 51_RIF20ST, and the 51_RSG20ST "Attrazione e retenzione di docenti di qualità" grant di Intesa Sanpaolo S.p.A. Stefano Taccheo is also deeply grateful to Prof. Orazio Svelto for inspiration and for introducing him to the laser field.

Thomas G. Mayerhofer and Juergen Popp gratefully acknowledge financial support from the European Union, the Thüringer Ministerium für Wirtschaft, Wissenschaft und Digitale Gesellschaft, the Thüringer Aufbaubank, the Federal Ministry of Education and Research (BMBF), the German Research Foundation (DFG), the Fonds der Chemischen Industrie, and the Carl Zeiss Foundation. Badhise Ben Bakir and Maeva Doron gratefully acknowledge support from Horizon-Europe Framework Programme with the project MILADO, CEA, CEA-Leti, the French Public Authorities and the French National Research Agency.

Optical Materials EXPRESS

Disclosures. The authors declare that there are no conflicts of interest related to this article.

Data availability. Data underlying the results presented in this paper are not publicly available at this time but may be obtained from the authors upon reasonable request.

References

1. https://www.iso.org/standard/39482.html
2. R. W. Waynant, I. K. Ilev, and I. Gannot, "Mid–infrared laser applications in medicine and biology," Phil. Trans of the Royal Soc. A **359**(1780), 635–644 (2001).
3. J. Morris, "Microfabrication of photonic devices for mid-infrared optical applications," PhD Thesis, 2018, http://hdl.handle.net/10399/4000
4. J. Hodgkinson and R. P. Tatam, "Optical gas sensing: A review," Meas. Sci. Technol. **24**(1), 012004 (2013).
5. D. Weidmann, F. K. Tittel, T. Aellen, *et al.*, "Mid-infrared trace-gas sensing with a quasi-continuous-wave Peltier-cooled distributed feedback quantum cascade laser," Appl. Phys. B: Lasers Opt. **79**(7), 907–913 (2004).
6. A. I. Lopez-Lorente and B. Mizaikoff, "Mid-infrared spectroscopy for protein analysis: potential and challenges," Anal Bioanal. Chem. **408**(11), 2875–2889 (2016).
7. M. A. Butt, M. Juchniewicz, M. Słowikowski, *et al.*, "Mid-infrared photonic sensors: exploring fundamentals, advanced materials, and cutting-edge applications," Sensors **25**(4), 1102 (2025).
8. S. C. Whiteman, Y. Yang, J. M. Jones, *et al.*, "FTIR spectroscopic analysis of sputum: Preliminary findings on a potential novel diagnostic marker for COPD," Therapeutic Advances in Respiratory Disease **2**(1), 23–31 (2008).
9. C. D. Santos Marfran, L. M. Morais Camilo, and M. G. Lima Kássio, "ATR-FTIR spectroscopy for virus identification: A powerful alternative," Journal of Biomedical Spectroscopy and Imaging **9**(3-4), 103–118 (2021).
10. S. Roy, D. Perez-Guaita, S. Bowden, *et al.*, "Spectroscopy goes viral: Diagnosis of hepatitis B and C virus infection from human sera using ATR-FTIR spectroscopy," Clinical Spectroscopy **1**, 100001 (2019).
11. V. G. Barauna, M. N. Singh, L. L. Barbosa, *et al.*, "Ultra-rapid on-site detection of SARS-CoV-2 infection using simple ATR-FTIR spectroscopy and analysis algorithm: high sensitivity and specificity," Anal. Chem. **93**(5), 2950–2958 (2021).
12. R. Tabaraki and F. Nazar, "Vancomycin-modified nitrogen and chloride doped carbon dots and their application as a Staphylococcus aureus probe," Anal. Chim. Acta **1268**, 341311 (2023).
13. V. Deckert, T. Deckert-Gaudig, D. Cialla-May, *et al.*, "Laser spectroscopic technique for direct identification of a single virus I: FASTER CARS," Proc. Natl. Acad. Sci. U.S.A. **117**(45), 27820–27824 (2020).
14. C. Petersen, U. Møller, I. Kubat, *et al.*, "Mid-infrared supercontinuum covering the 1.4–13.3 μm molecular fingerprint region using ultra-high NA chalcogenide step-index fibre," Nat. Photonics **8**(11), 830–834 (2014).
15. S. Vasilyev, I. Moskalev, V. Smolski, *et al.*, "Multi-octave visible to long-wave IR femtosecond continuum generated in Cr:ZnS-GaSe tandem," Opt. Express **27**(11), 16405–16412 (2019).
16. Q. Liu, *Portable and Wearable Sensing Systems: Techniques, Fabrication, and Biochemical Detection* (John Wiley & Sons: 2024).
17. R. Ballarini and S. Taccheo, "(Invited) Flexible photonics for biomedical applications: A review," Optical Materials: X **20**, 100265 (2023).
18. T. Hu, B. Dong, X. Luo, *et al.*, "Silicon photonic platforms for mid-infrared applications [Invited]," Photonics Res. **5**(5), 417–430 (2017).
19. M. Lepage, M. Chobé, S. Messaoudene, *et al.*, "Hybrid III–V/Si distributed-feedback quantum cascade lasers on a silicon-on-nitride platform," Opt. Express **33**(18), 37614 (2025).
20. T. Yokota, T. Nakamura, H. Kato, *et al.*, "A conformable imager for biometric authentication and vital sign measurement," Nat. Electron. **3**(2), 113–121 (2020).
21. A. Moin, A. Zhou, A. Rahimi, *et al.*, "A wearable biosensing system with in-sensor adaptive machine learning for hand gesture recognition," Nat. Electron. **4**(1), 54–63 (2020).
22. T. J. Wijaya, N. Higashitarumizu, S. Wang, *et al.*, "Mechanically flexible mid-wave infrared imagers using black phosphorus ink films," Nat. Commun. **16**(1), 5972 (2025).
23. H. Kim, S. Z. Uddin, D.-H. Lien, *et al.*, "Actively variable-spectrum optoelectronics with black phosphorus," Nature **596**(7871), 232–237 (2021).
24. Q. Guo, A. Pospischil, M. Bhuiyan, *et al.*, "Black phosphorus mid-infrared photodetectors with high gain," Nano Lett. **16**(7), 4648–4655 (2016).
25. Z. Lin, Y. Liu, U. Halim, *et al.*, "Solution-processable 2D semiconductors for high performance large-area electronics," Nature **562**(7726), 254–258 (2018).
26. M. Wuttig, H. Bhaskaran, and T. Taubner, "Phase-change materials for non-volatile photonic applications," Nat. Photonics **11**(8), 465–476 (2017).
27. Z. L. Sámson, K. F. MacDonald, F. De Angelis, *et al.*, "Metamaterial electro-optic switch of nanoscale thickness," Appl. Phys. Lett. **96**(14), 143105 (2010).
28. D. Kavungal, P. Magalhães, S. T. Kumar, *et al.*, "Artificial intelligence–coupled plasmonic infrared sensor for detection of structural protein biomarkers in neurodegenerative diseases," Sci. Adv. **9**(28), eadg9644 (2023).
29. J. Faist, F. Capasso, D. L. Sivco, *et al.*, "Quantum cascade laser," Science **264**(5158), 553–556 (1994).
30. R. F. Kazarinov and R. A. Suris, "Possibility of the amplification of electromagnetic waves in a semiconductor with a superlattice," Sov. Phys. Semi-Cond. **5**(4), 707–709 (1971).

Optical Materials EXPRESS

31. M. Beck, D. Hofstetter, T. Aellen, *et al.*, "Continuous wave operation of a mid-infrared semiconductor laser at room temperature," Science **295**(5553), 301–305 (2002).
32. M. S. Vitiello, G. Scalari, B. Williams, *et al.*, "Quantum cascade lasers: 20 years of challenges," Opt. Express **23**(4), 5167–5182 (2015).
33. G. Scalari and J. Faist, "30 years of the quantum cascade laser," Commun. Phys. **7**(1), 394 (2024).
34. M. Razeghi, Y. Bai, and F. Wang, "High-power, high-wall-plug-efficiency quantum cascade lasers with high-brightness in continuous wave operation at 3–300μm," Light: Sci. Appl. **14**(1), 252 (2025).
35. C. Y. Wang, L. Kuznetsova, V. M. Gkortsas, *et al.*, "Mode-locked pulses from mid-infrared quantum cascade lasers," Opt. Express **17**(15), 12929–12943 (2009).
36. A. Hugi, G. Villares, S. Blaser, *et al.*, "Mid-infrared frequency comb based on a quantum cascade laser," Nature **492**(7428), 229–233 (2012).
37. G. Marschick, M. David, X. Gsodam, *et al.*, "Micro-mirror aided mid-infrared plasmonic beam combiner monolithically integrated with quantum cascade lasers and detectors," Nanophotonics **14**(21), 3397–3405 (2025).
38. H. Nguyen-Van, A. N. Baranov, Z. Loghmari, *et al.*, "Quantum cascade lasers grown on silicon," Sci. Rep. **8**(1), 7206 (2018).
39. J. G Coutard, M. Brun, M. Fournier, *et al.*, "Volume Fabrication of Quantum Cascade Lasers on 200 mm-CMOS pilot line," Sci. Rep. **10**(1), 6185 (2020). https://www.nature.com/articles/s41598-020-63106-4
40. E. Commission, "Mid-infrared Wearable for Non-invasive biomarker monitoring," Available online: https://cordis.europa.eu/project/id/101115476
41. J.-G. Coutard, R. Aidam, F. Bernet, *et al.*, "Neogly QCL-based NI-CGM medical device," Biophotonics in Exercise Science, Sports Medicine, Health Monitoring Technologies, and Wearables V **12838**, 1 (2024).
42. J. Dong and J. W Tomlinson, "Lessons to learn from the 2024 NICE guideline on adrenal insufficiency," The Lancet Diabetes & Endocrinology **12**(12), 872–873 (2024).
43. G. Meyer, A. Hackemann, J. Reusch, *et al.*, "Nocturnal hypoglycemia identified by a continuous glucose monitoring system in patients with primary adrenal insufficiency (Addison's Disease)," Diabetes Technol. Ther. **14**(5), 386–388 (2012).
44. T. Wasilewski, W. Kamysz, and J. Gębicki, "AI-assisted detection of biomarkers by sensors and biosensors for early diagnosis and monitoring," Biosensors **14**(7), 356 (2024).
45. H. Zhou, D. Li, and C. Lee, "Technology Landscape Review of In-Sensor Photonic Intelligence: From Optical Sensors to Smart Devices," AI Sensors **1**(1), 5 (2025).
46. M. C. Yu, P. Rich, L. Foreman, *et al.*, "Label Free Detection of Sensitive Mid-Infrared Biomarkers of Glomerulonephritis in Urine Using Fourier Transform Infrared Spectroscopy," Sci. Rep. **7**(1), 4601 (2017).
47. B. Singh and J. Levy, "Biomedical Photonic Sensors: Enhancing Healthcare, Medical Diagnosis, Monitoring and Treatments," In Photonic Sensors for Biomedical Applications; Apple Academic Press 45–68 (2025).
48. N. Thanjavur, L. Bugude, and Y.-J. Kim, "Integration of functional materials in photonic and optoelectronic technologies for advanced medical diagnostics," Biosensors **15**(1), 38 (2025).
49. C. Kim, C. Favazza, and L. V. Wang, "In vivo photoacoustic tomography of chemicals: high-resolution functional and molecular optical imaging at new depths," Chem. Rev. **110**(5), 2756–2782 (2010).
50. S. Mallidi, G. P. Luke, and S. Emelianov, "Photoacoustic imaging in cancer detection, diagnosis, and treatment guidance," Trends Biotechnol. **29**(5), 213–221 (2011).
51. L. Lin and L. V. Wang, "The emerging role of photoacoustic imaging in clinical oncology," Nat. Rev. Clin. Oncol. **19**(6), 365–384 (2022).
52. A. Pérez-Pacheco, R. G. Ramírez-Chavarría, R. M. Quispe-Siccha, *et al.*, "Dynamic modeling of photoacoustic sensor data to classify human blood samples," Med. Biol. Eng. Comput. **62**(2), 389–403 (2024).
53. J. J. Riksen, A. V. Nikolaev, and G. van Soest, "Photoacoustic imaging on its way toward clinical utility: a tutorial review focusing on practical application in medicine," J. Biomed. Opt. **28**(12), 121205 (2023).
54. M. C. Lee, K. Landers, and J. Chan, "Activity-Based Photoacoustic Probes for Detection of Disease Biomarkers beyond Oncology," ACS Bio. Med. Chem. Au. **3**(3), 223–232 (2023).
55. X. Li, Y. W. Yew, J.S.Y. Lim, *et al.*, "Pilot study on photoacoustic imaging and confocal Raman spectroscopy-derived biomarkers for assessing structural and physiological skin changes in atopic dermatitis and metabolic diseases," Biomed. Opt. Express **16**(7), 2986–3000 (2025).
56. E. Hall, C. Tang, and L. Li, "Recent advancements in molecular photoacoustic tomography," JPhys Photonics **7**(3), 032003 (2025).
57. M. Huang, H. Yu, R. Gao, *et al.*, "Photoacoustic Imaging in Inflammatory Orthopedic Diseases: Progress toward Precise Diagnostics and Predictive Regulation," Adv. Sci. **12**(14), e2412745 (2025).
58. Digital biomarkers: From innovation to implementation. Available online: https://www.simon-kucher.com/en/insights/digital-biomarkers-innovation-implementation
59. F. Knieling, S. Lee, and V. Ntziachristos, "A primer on current status and future opportunities of clinical optoacoustic imaging," npj Imaging **3**(1), 4 (2025).
60. M. Perez-Liva, M. Alonso de Lecinana, M. Gutierrez-Fernandez, *et al.*, "Dual photoacoustic/ultrasound technologies for preclinical research: current status and future trends," Phys Med Biol **70**(7), 07TR01 (2025).

Optical Materials EXPRESS

61. K. Tangwanichgapong, P. Klanrit, P. Chatchawal, *et al.*, "Identification of molecular biomarkers in human serum for chronic kidney disease using attenuated total reflectance-Fourier transform infrared (ATR-FTIR) spectroscopy," Spectrochim Acta A Mol Biomol Spectrosc **334**, 125941 (2025).
62. A. Mishra, P. K. Gorai, P. Kaushal, *et al.*, "Infrared spectral analysis of gastrointestinal neuroendocrine tumors reveals diagnostic biomarkers," Sci. Rep. **15**(1), 24233 (2025).
63. C. Delrue, S. De Bruyne, and M. M. Speeckaert, "The Promise of Infrared Spectroscopy in Liquid Biopsies for Solid Cancer Detection," Diagnostics **15**(3), 368 (2025).
64. M. Schuler, G. Gerwert, M. Mann, *et al.*, "Alpha-synuclein misfolding as fluid biomarker for Parkinson's disease measured with the iRS platform," EMBO Mol. Med. **17**(6), 1203–1221 (2025).
65. Optics.org. Infrared spectroscopy allows population-level health screening. Available online: https://optics.org/news/15/7/38
66. N.M.L. Sciences, New screening tool uses infrared light and machine learning to detect multiple health conditions. Available online: https://www.news-medical.net/news/20240719/New-screening-tool-uses-infrared-light-and-machine-learning-to-detect-multiple-health-conditions.aspx
67. R. K. Upadhyay, "Emerging risk biomarkers in cardiovascular diseases and disorders," J. Lipids **2015**, 1–50 (2015).
68. Q. Zhang, Y. Xing, K. Wang, *et al.*, "Feasibility of non-invasive measurement of cardiac biomarkers using mid-infrared spectroscopy: finite element analysis and experimental validation," Analyst **150**(12), 2689–2701 (2025).
69. J. Haas and B. Mizaikoff, "Advances in Mid-Infrared Spectroscopy for Chemical Analysis," Annual Rev. Anal. Chem. **9**(1), 45–68 (2016).
70. C. Hughes and M. J. Baker, "Can mid-infrared biomedical spectroscopy of cells, fluids and tissue aid improvements in cancer survival? A patient paradigm," Analyst **141**(2), 467–475 (2016).
71. G. F. Rangel, L. D. de León Martínez, L. S. Walter, *et al.*, "Recent advances and trends in mid-infrared chem/bio sensors," TrAC Trends in Analytical Chemistry **180**, 117916 (2024).
72. J. F. da Silveira Petruci, D. da Silva Sousa, and B. Mizaikoff, "Advanced Mid-Infrared Sensors for Molecular Analysis," Anal. Chem. **97**(13), 6871–6890 (2025).
73. L. Leal, M. Nogueira, R. Canevari, *et al.*, "Vibration spectroscopy and body biofluids: Literature review for clinical applications," Photodiagn. Photodyn. Ther. **24**, 237–244 (2018).
74. S. G. Kazarian and K. L. Chan, "ATR-FTIR spectroscopic imaging: recent advances and applications to biological systems," Analyst **138**(7), 1940–1951 (2013).
75. R. Aerts, J. Bogaerts, C. Johannessen, *et al.*, "Vibrational Optical Activity Study of Four Antibiotic (Lipo)glycopeptides: Vancomycin, Oritavancin, Dalbavancin, and Teicoplanin," ACS Omega **7**(48), 43657–43664 (2022).
76. J. G. Kelly, J. Trevisan, A. D. Scott, *et al.*, "Biospectroscopy to metabolically profile biomolecular structure: a multistage approach linking computational analysis with biomarkers," J. Proteome Res. **10**(4), 1437–1448 (2011).
77. A. Manca, A. Palermiti, J. Mula, *et al.*, "A description of Cannabinoid levels in Cannabis oil by high-performance liquid chromatography-mass spectrometry in a reference laboratory of North-Italy," Phytomedicine **102**, 154218 (2022).
78. M. Hemdan, M. A. Ali, A. S. Doghish, *et al.*, "Innovations in biosensor technologies for healthcare diagnostics and therapeutic drug monitoring: applications, recent progress, and future research challenges," Sensors **24**(16), 5143 (2024).
79. V. Lifesciences, Quantificazione dei biomarcatori farmacodinamici: impatto dei farmaci e bioanalisi nello sviluppo di nuove entità chimiche. Available online: https://veedalifesciences.com/it/quantifying-pharmacodynamic-biomarkers-drug-impact-and-bioanalysis-in-new-chemical-entity-development/ (accessed on).
80. J.-H. Choi, I. Haizan, and J.-W. Choi, "Recent advances in two-dimensional materials for the diagnosis and treatment of neurodegenerative diseases," Discover Nano **19**(1), 151 (2024).
81. A. Karlas, M. A. Pleitez, J. Aguirre, *et al.*, "Optoacoustic imaging in endocrinology and metabolism," Nat. Rev. Endocrinol. **17**(6), 323–335 (2021).
82. Y. Jin, Y. Yin, C. Li, *et al.*, "Non-invasive monitoring of human health by photoacoustic spectroscopy," Sensors **22**(3), 1155 (2022).
83. G. Thenuwara, J. Curtin, and F. Tian, "Advances in diagnostic tools and therapeutic approaches for gliomas: a comprehensive review," Sensors **23**(24), 9842 (2023).
84. P. Bouguer, Essai d'Optique (1729).
85. J. H. Lambert and E. Anding, Lambert's photometrie: (photometria sive de mensura et gradibus luminis, colorum et umbrae). (1760). Heft 3, Tl. 6 und 7 - Anmerkungen (Engelmann, 1892).
86. Beer, "Bestimmung der Absorption des rothen Lichts in farbigen Flüssigkeiten," Ann. Phys. **162**(5), 78–88 (1852).
87. T. G. Mayerhöfer, S. Pahlow, J. Popp, *et al.*, "The Bouguer-Beer-Lambert Law: Shining Light on the Obscure," ChemPhysChem **21**(18), 2029–2046 (2020).
88. T. G. Mayerhöfer, *Wave Optics in Infrared Spectroscopy - Theory, Simulation and Modeling* (Elsevier, 2024).
89. A. Fresnel, "Ueber das Gesetz der Modificationen, welche die Reflexion dem polarisirten Lichte einprägt," Ann. Phys. **98**(5), 90–126 (1831).
90. J. C. Maxwell, "VIII. A dynamical theory of the electromagnetic field," Philos. Trans. R. Soc. London **155**, 459–512 (1865).

Optical Materials EXPRESS

91. H. A. Lorentz, "Ueber die Beziehung zwischen der Fortpflanzungsgeschwindigkeit des Lichtes und der Körperdichte," Ann. Phys. **245**(4), 641–665 (1880).
92. L. Lorenz, "Ueber die Refractionsconstante," Ann. Phys. **247**(9), 70–103 (1880).
93. M. Planck, "Über die Extinction des Lichtes in einem optisch homogenen Medium von normaler Dispersion," Sitzungsberichte der Königlich Preussischen Akademie der Wissenschaften I 740–750 (1904).
94. M. Born, *Principles of Optics: Electromagnetic Theory of Propagation, Interference and Diffraction of Light* (Cambridge University Press, 1999).
95. A. Bauer, O. Hertzberg, A. Küderle, *et al.*, "IR-spectroscopy of skin in vivo: Optimal skin sites and properties for non-invasive glucose measurement by photoacoustic and photothermal spectroscopy," J. Biophotonics **11**(1), e201600261 (2018).
96. T. G. Mayerhöfer, S. Pahlow, U. Hübner, *et al.*, "CaF2: An Ideal Substrate Material for Infrared Spectroscopy?" Anal. Chem. **92**(13), 9024–9031 (2020).
97. T. G. Mayerhöfer and J. Popp, "Understanding the Role of the Evanescent Field in Attenuated Total Reflection (ATR) Spectroscopy," Appl. Spectrosc. 00037028251358400 (2025).
98. T. G. Mayerhöfer, S. Pahlow, U. Hübner, *et al.*, "Removing interference-based effects from the infrared transflectance spectra of thin films on metallic substrates: a fast and wave optics conform solution," Analyst **143**(13), 3164–3175 (2018).
99. T. G. Mayerhöfer, S. Pahlow, U. Hübner, *et al.*, "Removing interference-based effects from infrared spectra – interference fringes re-revisited," Analyst **145**(9), 3385–3394 (2020).
100. T. G. Mayerhöfer, W. D. P. Costa, and J. Popp, "Sophisticated Attenuated Total Reflection Correction Within Seconds for Unpolarized Incident Light at 45°," Appl. Spectrosc. **78**(3), 321–328 (2024).
101. T. G. Mayerhöfer and J. Popp, "Understanding Advanced Attenuated Total Reflection Correction: The Low Absorbance Assumption," Appl. Spectrosc. **79**(2), 298–305 (2025).
102. T. G. Mayerhöfer and J. Popp, "Developing Correction Methods by Revisiting the Concept of Effective Thickness in Attenuated Total Reflection Spectroscopy," Appl. Spectrosc. **79**(3), 465–472 (2025).
103. T. G. Mayerhöfer and J. Popp, "Understanding and Employing (Non-)Linearities in Attenuated Total Reflection Spectroscopy," Appl. Spectrosc. **79**(8), 1290–1296 (2025).
104. T. G. Mayerhöfer, O. Ilchenko, A. Kutsyk, *et al.*, "Beyond Beer's Law: Quasi-Ideal Binary Liquid Mixtures," Appl. Spectrosc. **76**(1), 92–104 (2022).
105. R. Kramer, *Chemometric Techniques for Quantitative Analysis* (CRC Press, 1998).
106. H. Mark and J. Workman, *Chemometrics in Spectroscopy*: Revised Second Edition (Academic Press, 2021).
107. A. Olivieri, *Introduction to Multivariate Calibration: A Practical Approach* (Springer International Publishing, 2024).
108. T. G. Mayerhöfer, O. Ilchenko, A. Kutsyk, *et al.*, "Complex-Valued Chemometrics in Spectroscopy: Classical Least Squares Regression," Appl. Spectrosc. **79**(12), 1768–1775 (2025).
109. T. G. Mayerhöfer, O. Ilchenko, A. Kutsyk, *et al.*, "Complex-valued Chemometrics in Spectroscopy: Inverse Least Square Regression," Appl. Spectrosc. **80**(1), 100–108 (2026).
110. T. G. Mayerhöfer, O. Ilchenko, A. Kutsyk, *et al.*, "Complex-valued Chemometrics in Spectroscopy: Principal Component Regression," Appl. Spectrosc. 00037028251393273 (2025).
111. T. G. Mayerhöfer, O. Ilchenko, A. Kutsyk, *et al.*, "Complex-valued Chemometrics in Spectroscopy: Partial Least Squares Regression," 0, 00037028251401941 (2025).
112. S. Guo, T. Mayerhöfer, S. Pahlow, *et al.*, "Deep learning for 'artefact' removal in infrared spectroscopy," Analyst **145**(15), 5213–5220 (2020).
113. A. Mokari, S. Guo, and T. Bocklitz, "Exploring the Steps of Infrared (IR) Spectral Analysis: Pre-Processing, (Classical) Data Modelling, and Deep Learning," Molecules **28**(19), 6886 (2023).
114. X. Chen, Q. Chai, N. Lin, *et al.*, "1D convolutional neural network for the discrimination of aristolochic acids and their analogues based on near-infrared spectroscopy," Anal. Methods **11**(40), 5118–5125 (2019).
115. L. Zhang, X. Ding, R. Hou, *et al.*, "Classification Modeling Method for Near-Infrared Spectroscopy of Tobacco Based on Multimodal Convolution Neural Networks," Journal of Analytical Methods in Chemistry **2020**, 1–13 (2020).
116. P. R. Wiecha, A. Arbouet, C. Girard, *et al.*, "Deep learning in nano-photonics: inverse design and beyond," Photonics Res. **9**(5), B182–B200 (2021).
117. F. L. Teixeira, C. Sarris, Y. Zhang, *et al.*, "Finite-difference time-domain methods," Nat. Rev. Methods Primers **3**(1), 75 (2023).
118. B. Ben Bakir, "Group III–V on Silicon: A Brand-New Optoelectronics," in *Nanodevices for Photonics and Electronics* (Jenny Stanford Publishing 2016).
119. A. Spott, J. Peters, M. L. Davenport, *et al.*, "Heterogeneous integration of mid-infrared quantum cascade lasers on silicon," Optica **3**(5), 545–552 (2016).
120. M. W. Sigrist, "Trace gas monitoring by laser photoacoustic spectroscopy and related techniques (plenary)," Rev. Sci. Instrum. **74**(1), 486–490 (2003).
121. A. Miklos, P. Hess, and Z. Bozóki, "Application of Acoustic Resonators in Photoacoustic Trace Gas Analysis and Metrology," Rev. Sci. Instrum. **72**(4), 1937–1955 (2001).

Optical Materials EXPRESS

122. V. Zéninari, A. V. Kapitanov, D. Courtois, *et al.*, "Design and characteristics of a differential Helmholtz resonant PA cell for infrared gas detection," Infrared Phys. Technol. **40**(1), 1–23 (1999).
123. J. Glière, M. Rouxel, B. Brun, *et al.*, "Challenges in the design and fabrication of a lab-on-a-chip photoacoustic gas sensor," Sensors **14**(1), 957–974 (2014).
124. A. Gliere, P. Barritault, A. Berthelot, *et al.*, "Downsizing and Silicon Integration of Photoacoustic Gas Cells," Int. J. Thermophys. **41**(2), 16 (2020).
125. G. Wysocki, "Influence of molecular relaxation dynamics on quartz-enhanced photoacoustic detection of CO2 at λ=2 μm," Appl. Phys. B **85**(2-3), 301–306 (2006).
126. H. Yi, O. Laurent, and S. Schilt, "Simultaneous Monitoring of Atmospheric CH_4, N_2O, and H_2O Using a Single Gas Sensor Based on Mid-IR Quartz-Enhanced Photoacoustic Spectroscopy," Anal. Chem. **94**(50), 17522–17532 (2022).
127. World Health Organization. Global Report On Diabetes. at https://www.who.int/publications/i/item/9789241565257 (2016).
128. B. Zhou, A. Rayner, E. Gregg, *et al.*, "Worldwide trends in diabetes prevalence and treatment from 1990 to 2022: a pooled analysis of 1108 population-representative studies with 141 million participants," The Lancet **404**(10467), 2077–2093 (2024).
129. J. L. Smith, The Pursuit of Noninvasive Glucose: "Hunting the Deceitful Turkey" By John L. Smith.
130. M. Kim, "The Quest for Noninvasive Glucose Monitoring," Opt. Photonics News **33**(10), 30–37 (2022).
131. R. Henn, C. G. Kirchler, Z. L. Schirmeister, *et al.*, "Hemodialysis monitoring using mid- and near-infrared spectroscopy with partial least squares regression," J. Biophotonics **11**(7), e201700365 (2018).
132. A. Rosencwaig and A. Gersho, "Theory of the photoacoustic effect with solids," J. Appl. Phys. **47**(1), 64–69 (1976).
133. A. C. Tam, "Applications of photoacoustic sensing techniques," Rev. Mod. Phys. **58**(2), 381–431 (1986).
134. J. Kottmann, J. M. Rey, and M. W. Sigrist, "Mid-Infrared Photoacoustic Detection of Glucose in Human Skin: Towards Non-Invasive Diagnostics," Sensors **16**(10), 1663 (2016).
135. M. A. Pleitez, T. Lieblein, A. Bauer, *et al.*, "In Vivo Noninvasive Monitoring of Glucose Concentration in Human Epidermis by Mid-Infrared Pulsed Photoacoustic Spectroscopy," Anal. Chem. **85**(2), 1013–1020 (2013).
136. J. Y. Sim, C.-G. Ahn, E.-J. Jeong, *et al.*, "In vivo Microscopic Photoacoustic Spectroscopy for Non-Invasive Glucose Monitoring Invulnerable to Skin Secretion Products," Sci. Rep. **8**(1), 1059 (2018).
137. M. A. Pleitez, O. Hertzberg, A. Bauer, *et al.*, "Photothermal deflectometry enhanced by total internal reflection enables non-invasive glucose monitoring in human epidermis," Analyst **140**(2), 483–488 (2015).
138. N. Uluç, S. Glasl, F. Gasparin, *et al.*, "Non-invasive measurements of blood glucose levels by time-gating mid-infrared optoacoustic signals," Nat. Metab. **6**(4), 678–686 (2024).